Sonseca, A.; Camarero-Espinosa, S.; Peponi, L.; Weder, C.; Foster, E.; Kenny, JM.; Giménez Torres, E. (2014). Mechanical and Shape-Memory Properties of Poly(mannitol sebacate)/Cellulose Nanocrystal Nanocomposites. Journal of Polymer Science Part A Polymer Chemistry. 52(21):3123-3133. https://doi.org/10.1002/pola.27367

Journal of Polymer Science, Part A: Polymer Chemistry

Mechanical and shape-memory properties of poly(mannitol sebacate) / cellulose nanocrystal nanocomposites

Journal:	*Journal of Polymer Science, Part A*
Manuscript ID:	JPOL-A-14-0463.R2
Wiley - Manuscript type:	Original Article
Keywords:	nanoparticles < N, nanocomposites < N, mechanical properties < M, Poly(polyol sebacate), cellulose nanocrystals, shape memory

Mechanical and shape-memory properties of poly(mannitol sebacate) / cellulose nanocrystal nanocomposites

Águeda Sonseca[1*], Sandra Camarero-Espinosa[2], Laura Peponi[3], Christoph Weder[2], E. Johan Foster[2], José M. Kenny[3], and Enrique Giménez[1]

[1]Instituto de Tecnología de Materiales, Universidad Politécnica de Valencia (UPV), Camino de Vera s/nº, 46022 Valencia (Spain)

[2]Adolphe Merkle Institute, University of Fribourg, Rte de l´Ancienne Papeterie, CH-1723 Marly (Switzerland)

[3]Instituto de Ciencia y Tecnología de Polímeros (ICTP-CSIC), Juan de la Cierva 3, 28006 Madrid (Spain)

***To whom all correspondence should be addressed. Phone number; (+34)963879625; e-mail address; agsonol@posgrado.upv.es**

Abstract

Polyesters based on polyols and sebacic acid, known as poly(polyol sebacate)s (PPS), are attracting considerable attention, as their properties are potentially useful in the context of soft-tissue engineering applications. To overcome the drawback that PPSs generally display rather low strength and stiffness, we have pursued the preparation of nanocomposites based poly(mannitol sebacate) (PMS), a prominent example of this materials family, with cellulose nanocrystals (CNCs). Nanocomposites were achieved in a two-step process. A soluble, low-molecular-weight PMS pre-polymer was formed via the polycondensation reaction between sebacic acid and D-mannitol. Nanocomposites with different CNC content were prepared by

solution-casting and curing under vacuum using two different profiles designed to prepare materials with low and high degree of crosslinking. The as-prepared nanocomposites have higher stiffness and toughness than the neat PMS matrix while maintaining a high elongation at break. A highly crosslinked nanocomposite with a CNC content of 5 wt% displays a 6-fold increase in Young´s modulus and a 5-fold improvement in toughness. Nanocomposites also exhibit a shape memory effect with a switch temperature in the range of 15-45 ºC; in particular the materials with a thermal transition in the upper part of this range are potentially useful for biomedical applications.

Keywords: Poly(polyol sebacate), cellulose nanocrystals, nanocomposites, nanoparticles, mechanical properties, shape memory.

Introduction

Synthetic polyester elastomers have received extensive attention in the past few years because of their stable network structure, elastic properties, biodegradability under physiological conditions and biocompatibility with response of the host tissue similar to PLA and PLGA resulting in formation of thinner fibrous capsules as well as lower inflammatory response.[1, 2] Several polyester elastomers based on polyols such as 1,8-octanediol, ethylene glycol, butylene glycol or glycerol, and carboxylic acids such as citric and sebacic acid,[3-7] have been considered for soft tissue engineering applications such a nerve-guidance, drug delivery, tissue adhesives and scaffolds to repair or replace body tissues.[8-11] After Wang and coworkers[12] first reported crosslinked poly(glycerol sebacate) (PGS) elastomers, several other polyols have been used

instead of glycerol to expand the properties of the family of poly(polyol sebacate)s (PPS)[1]. Attractive features of PPS are that they are based on inexpensive, non-toxic monomers and that their mechanical properties can be readily tuned through the choice of the polyol, the monomer ratio, and the polycondensation conditions. Nevertheless, the spectrum of mechanical properties (tensile strength and elastic modulus) that can be achieved without compromising their elasticity is limited.[1, 13] This limits their use even in some soft tissue engineering applications in which the tissue involved is at the same time stiffer (Young's modulus = 0.7-250 MPa) and more elastic (elongation at break > 10%) than representatives members of the PPS family, such skin, nerves, cartilage, heart valves, and tendons.[14-16] Their usefulness is thus limited in applications where high strength and high flexibility are required, such as ligating rubber bands for blood vessels, elastomeric sutures, flexible coatings for stents, surgical devices, vascular grafts, surgical wound dressings, or catheters and small diameter tubes for drainage.[17] The addition of reinforcing fillers has proven to be an effective approach to increase the strength and stiffness of a given polymer, but normally these improvements come at the expense of a reduction of the elasticity. Most of the approaches to create PPS composites are based on the introduction of inorganic components such halloysiste nanotubes (clays) or multi-walled carbon nanotubes (MWCNTs).[18-20] In the last decade, composite materials based on nanocellulose have been the base of research efforts because the fact that natural cellulosic materials are abundant, inexpensive, renewable, biodegradable under certain conditions, and exhibit generally low toxicity.[21, 22] Cellulose nanocrystals (CNCs)[23-26] might be a particularly interesting filler to reinforce low-modulus PPS matrices, as they exhibit high stiffness (elastic modulus ~ 143 GPa) and high aspect ratio (with diameters of ~5-50 nm and lengths of 100-3000 nm depending on the source).[27-29] Compared with other nanofillers such as clays or bioceramics (Bioglass®), CNCs have superior specific

properties.[27, 30] The specific Young´s modulus of commercial Bioglass® is ~ 13 GPa cm^3/g and for clays ~ 55 GPa cm^3/g while the value for CNC, is ~100 GPa cm^3/g due to its low density.[31-34] Multi-walled carbon nanotubes MWCNTs have a higher specific modulus than CNCs, but the latter have an established manufacturing process and likely lower cost apart from significantly lower toxicity.[22, 35, 36] In addition, the presence of abundant hydroxyl groups on the CNC surface is expected to promote a uniform dispersion of the filler in the PMS matrix investigated through a strong affinity or reaction with the hydroxyl and carboxyl functional groups in the polymer backbone.[37] Here we show that the PMS/CNCs nanocomposites exhibit a higher stiffness and toughness than the neat PMS matrix while a high elongation at break is maintained. We further demonstrate that their property matrix makes the new nanocomposites useful as biomedical shape-memory polymers (SMPs); in particular the increased mechanical energy that can be stored in the temporary shape is useful,[38] as it permits to exert force enabling better shape recovery in complicated or restricted environments where displacement of the surrounding tissue is required. Based on this enhancement of the rubbery modulus region observed, we also investigated the thermal induced shape memory properties of these materials.

Experimental section

Materials. Deuterated dimethylsulfoxide (DMSO- d_6), dimethylformamide (DMF), sulfuric acid, sebacic acid (SA) (99% purity), and D-mannitol (MA) (99% purity), were purchased from Sigma Aldrich. Hydrochloric acid (HCl, 37% reagent grade) and sodium hydroxide (NaOH, 98% reagent grade) were purchased from Scharlau. Ultrapure water was directly taken from a Sartorius Stedim Arium 611 VF® water purification system (ρ = 18.2 mΩ·cm). Cellulose

nanocrystals were isolated from cotton (Whatman No.1 filter paper) by controlled hydrolysis with sulphuric acid according to a protocol[39] that is a modification of the method originally described by Dong et al.[40] The protocol introduces a small concentration of sulfate ester groups on the surface of the CNCs, which help to form stable suspensions in polar solvents.[41]

Isolation and Properties of CNCs. CNCs were isolated from cotton using a previously reported protocol.[39] TEM analysis of the CNC suspension after sulphuric acid hydrolysis revealed a needle-like structure. Dimensions and aspect ratio (length:width) of the CNCs were determined by analysis of several TEM images (**Supporting Figures S1 and S2**) resulting in an average width of 18±2 nm, an average length of 199±14 nm, and an average aspect ratio of 11±1 (**Supporting Table S2**). The apparent crystallinity of the CNCs was calculated from X-ray diffraction (XRD) patterns. The crystal structure of the CNCs is cellulose I, and the apparent crystallinity was determined to be 69% (**Supporting Figure S3**). The concentration of the surface charges present as sulfate groups on the surface of the CNCs was determined by conductometric titration. This experiment revealed a sulfate content of 91±4 mM/$kg_{cellulose}$ (**Supporting Figure S4**), which is in accordance with previously reported values.[42]

Synthesis of poly(mannitol sebacate) (PMS) pre-polymer. Sebacic acid (SA) and mannitol (MA) were reacted as described previously.[1] Equimolar amounts (0.068 mol) of SA (13.79 g) and MA (12.42 g) were charged into a 250 mL three-necked round-bottom flask equipped with a stirrer and a condenser, which was placed in an oil heating bath and purged during 0.5 h with nitrogen. The temperature was slowly increased to 150 °C under continuous stirring and nitrogen flow to produce approximately 20 g of the pre-polymer (**Scheme 1**). The reaction was stopped after 13 h (1 h before gelation occurs), and the pre-polymer was dissolved in DMF (150 mg/mL), filtered and purified by dropwise precipitation into a 4-fold excess of cold ultrapure water under

continuous stirring. The precipited pre-polymer was collected and dried under vacuum until no more solvent was detected in the infrared spectra. The yield of the reaction was ~82%, as calculated from the weight of the monomers before reaction and the weight of the obtained pre-polymer after reaction.

Characterization of PMS pre-polymer. The number-average molecular weight (M_n), weight-average molecular weight (M_w), and polydispersity index (PDI) of the PMS pre-polymer were determined by gel permeation chromatography (GPC). The experiment was conducted on a series 1200 HPLC system (Agilent Technologies) equipped with a Polymer Laboratories PLgel 5 μm mixed-C column and two detection systems: a multi-angle laser light scattering (MALLS, miniDAWN^{TM} TREOS) (λ = 658 nm, 25 °C) and a refractive index (RI, Optilab REX) (λ = 658 nm, 40 °C) detector. The sample concentration was ~2 mg/mL and THF was used as eluent at 40 °C (flow rate, 1.0 mL/min). The chromatogram was processed with Wyatt Technology software (ASTRA). The incremental refractive index (d*n*/d*c*) was estimated by a single-injection method that assumed 100% mass recovery from the columns. The GPC analysis resulted an M_n = 6180 g/mol and M_w = 7501 g/mol (**Supporting Table S1**). The ^{1}H-NMR spectrum of the PMS pre-polymer was acquired in DMSO-d_6 on a Varian Mercury VX-300 MHz NMR spectrometer (**Supporting Figure S5**). The composition was determined from the ratio of the integrals of the signals associated with the mannitol and sebacic acid peaks[1] revealing an incorporation of approximately equimolar amounts of the monomers into the pre-polymer.

Preparation of PMS/CNC nanocomposites. The pre-polymer was first dissolved in DMF (100 mg/mL) by stirring for 4 h. Suspensions of CNCs at concentration of 10 mg/mL were prepared at appropriate ratio in DMF(designed to combine with 1.5 g of dry pre-polymer and form 1 wt%, 5 wt% and 10 wt% of PMS/CNC nanocomposites) by 40 min of ultrasonic treatment in a horn

sonicator (Q500 sonicator, QSonica, 20kHz/500Watts, fitted with a ¼" microtip probe) with 1 sec on/off pulse conditions at a 20% of amplitude. CNC suspensions were stirred with PMS pre-polymer/DMF solution for 30 min and cast into aluminium Petri dishes (93 x 7 mm) and allowed to dry in an oven at 70 °C. Films consisting of the neat pre-polymer only, were prepared for reference purposes under the same conditions. The resulting pre-polymer/nanocomposite and the neat pre-polymer films were placed in a vacuum oven for further reaction. Two different curing profiles were applied, in which temperature and duration of the thermal treatment were varied to obtain samples with low and high degree of crosslinking. Samples with low degree of crosslinking were maintained at 120 °C for 72 hours under vacuum (60 cm Hg). Samples with high degree of crosslinking were obtained by using the same protocol and subsequently increasing the temperature to 170 °C while maintaining the vacuum (60 cm Hg) for a further 24 hours. Both procedures afforded films of ~ 150-200 μm of thickness.

Fourier Transform Infrared Spectroscopy (FTIR). FTIR transmission spectra were recorded for all samples using a Thermo Nicolet 5700 spectrometer between 500-4500 cm^{-1} with a 4 cm^{-1} resolution and an Attenuated Total Reflectance (ATR) cell. Backgrounds were acquired before every 3rd sample. All samples were vacuum-dried before measurement.

Transmission Electron Microscopy (TEM). A Phillips CM10 microscope with an accelerating voltage of 80 kV was used to record TEM micrographs of thin cross sections of the composites. Thin cross sections (thickness 3-10 μm) were cut under cryogenic conditions using a Leica CM1950 cryostat; they were stained with 2% aqueous uranyl acetate on carbon-coated copper grids.[43]

Mechanical Micro-Testing. The elongation at break, Young´s modulus and ultimate tensile strength were analyzed by mechanical tensile tests carried out on a DEBEN microtester equipped with a 150 N load cell and operated at a crosshead speed of 0.4 mm/min at room temperature. Specimen dimensions were typically 15 x 4 mm x 150~200 µm. The Young´s modulus (E) was determined from the initial slope of the stress-strain curves in the strain range of 0-10% for samples with low degree of crosslinking and 0-5% for samples with high degree of crosslinking. For each sample, a minimum of 5 rectangular samples were tested and the mechanical data were averaged.

Dynamic Mechanical Thermal Analysis (DMTA) and thermally activated shape memory properties. The mechanical behaviour as a function of temperature was characterized by DMTA measurements on a TA Q800 instrument (TA instruments). Samples were cut into 30 x 4 mm x 150~200 µm rectangular shapes and tested in tensile mode with a temperature ramp method from -50 to 150 °C at a heating rate of 3 °C/min. Frequency and strain amplitude were kept constant at 1 Hz and 15 µm, respectively. Glass transition temperatures were calculated as the maximum in tangent delta peak. Shape-memory characteristics of the samples were quantified by cyclic, thermomechanical tensile tests in the DMTA. The experiment involved the creation of a temporary shape in a programming mode and a free stress recovery step of the permanent shape. The programming mode was performed under strain-controlled conditions in three steps: (1) the sample was equilibrated at 45 °C for 10 min before a force ramp of 3 N/min was applied until a strain of 30% was reached. (2) While the stress was kept constant, the sample was subsequently cooled to 15 °C. (3) The sample was unloaded to zero stress and the temperature was maintained at 15 °C for 5 min to ensure the fixation of the temporary shape. At this point, the recovery step was initiated by increasing the temperature to 45 °C, which was then maintained for 20 min. All

samples were tested for 3 or 4 cycles. The ability to fix the temporary shape at 15 °C (shape fixity ratio, R_f) and the ability to recover the permanent shape at 45 ºC (shape recovery ratio, R_r) were quantified using the following equations:[44-46]

$$R_f\ (N) = \frac{\varepsilon_u\ (N)}{\varepsilon_m\ (N)} x100\% \quad (1)$$

$$R_r\ (N) = \frac{\varepsilon_m\ (N) - \varepsilon_f\ (N)}{\varepsilon_m\ (N) - \varepsilon_f\ (N-1)} x100\% \quad (2)$$

where ε_m is the maximum strain achieved in the Nth cycle after cooling and before unloading, ε_u is the fixed strain after unloading the sample at 15 °C in the same cycle, and ε_f is the residual strain of the sample after the recovery step. Samples with high degree of crosslinking conditions were also tested using a programming temperature of 60 ºC. Should be pointed out that the shape memory temperature profiles where selected taking in account the results obtained in the DMTA analysis and to fulfil the requirements for future biomedical applications in terms to facilitate the manipulation, storage and implantation of a possible device. Shape memory biomedical devices are recommended to be activated in the range of 36-55 ºC, being also desirable the possibility to avoid premature activation retaining the shape at room temperature.[47]

Results and discussion

Synthesis of the PMS prepolymer and its nanocomposites with CNCs. The preparation of the PMS/CNC nanocomposites was achieved in a two-step process. First, a soluble, low-molecular-weight PMS pre-polymer was formed via the polycondensation reaction between sebacic acid and D-mannitol (**Scheme 1**). In this first stage, the esterification is preferentially dominated by the reaction of the primary hydroxyl groups from D-mannitol (situated at two ends) with

carboxylic acid groups from sebacic acid.[48, 49] The reaction was stopped before gelation occurred, affording a polyester with a number-average molecular weight, M_n of 6180 g/mol and a weight-average molecular weight, M_w of 7501 g/mol. Nanocomposites with 1 wt%, 5 wt% and 10 wt% CNCs were subsequently prepared by solution-casting mixtures of the PMS pre-polymer and the CNCs, and curing in a second step under vacuum using two different curing profiles designed to prepare materials with low and high degree of crosslinking. At this point, there is a lack of primary hydroxyl groups in the pre-polymer backbone resulting in a second stage dominated by the reaction of the secondary hydroxyl groups from D-mannitol with residual carboxylic acids from sebacic acid crosslinking the system. However, the addition of CNC to the system, introduces new hydroxyl groups that can offset the initial stoichiometry of OH/COOH groups. Given the surface chemistry of the CNC along with the presence of unreacted hydroxyl and carboxyl groups in the pre-polymer, when the system is heated, the new hydroxyl groups from the filler can participate and compete in ester formation and hydrogen bonding interactions with the pre-polymer chains becoming part of the network. To have an idea of how much the stoichiometry of the system can be modified **Table 1** shows an estimation of how the presence of CNCs affects the concentration of –OH groups introduced in each composite with the CNC addition (***Supporting Calculation Method M1***) increased from 6, 30 and 60 % for 1, 5 and 10 wt% of CNC respectively. The total amount of –OHs available on 1g of PMS matrix was estimated supposing an ideal linear pre-polymer with four available –OHs per mannitol molecule taking into account the molecular weight value obtained from GPC test. The total amount of –OHs available on the CNC introduced in each sample (1, 5 and 10 wt%) was estimated taking in account the molecular weight of native cellulose with 20% of the total –OHs as reactive sites.[50]

The morphology of the nanocomposites was investigated by transmission electron microscopy of cryo-microtomed samples. The micrograph shown in **Figure 2** corresponds to the highest filler ratio nanocomposite with high degree of crosslinking, and reveals well-dispersed CNCs in the PMS matrix. This sample is representative of the filler distribution along all the samples, since lower CNC contents are easy to disperse as they have lower trend to form aggregates, and in addition, the differences in the crosslinking profile are not expected to produce high differences in the dispersion of the filler as no solvent was present when the curing profiles were initiated. Furthermore, in order to confirm the ester formation and the presence of CNCs, ATR-FTIR spectra of the neat PMS matrix and the PMS/CNC nanocomposites prepared under low and high degree of crosslinking conditions were recorded. **Figure 1** shows parts of the spectra in which the most relevance bands are observable; the full IR-spectra are shown in **Supporting Figure S6**. For both curing conditions, the spectra of the neat PMS show the characteristic absorption bands for hydrogen-bonded hydroxyl groups (3500-3200 cm^{-1}) and for carbonyl stretching vibrations of the ester groups (1800-1600 cm^{-1}) in the polymer backbone, confirming the formation of polyesters. The bands around 2924 cm^{-1} and 2852 cm^{-1} are assigned to methylene (-CH_2-) groups for the diacid residue and are observed in all spectra. A peak close to 1150 cm^{-1} was assigned to the –CO stretch associated with the ester groups.[51] Samples prepared under low degree of crosslinking conditions show a broad and intense -OH stretch peak at 3350 cm^{-1}, an acid peak at 1705 cm^{-1}, and an ester peak at 1740 cm^{-1}, revealing a substantial fraction of unreacted hydroxyl and acid groups. Samples prepared under high degree of crosslinking conditions show a smaller absorption related to the hydroxyl groups at 3350 cm^{-1} and a more pronounced –CO stretch associated with the ester groups, indicating a higher degree of esterification. Inspection of the spectra of the nanocomposites reveal a similar picture; in the case

of nanocomposites with 5 and 10 wt% CNCs, peaks associated with the CNC–OH close to 3338 cm^{-1} can also be discerned.

Mechanical testing. To relate the incorporation of CNCs and the different curing conditions to the mechanical properties of the PMS matrix, micro-tensile tests were carried out. In both systems (samples with low and high degree of crosslinking), the introduction of CNCs led to an improvement of the Young´s modulus and tensile strength, which increase with the CNC content (**Table 2**, **Figure 3**). Also the elongation at break and toughness increased up to a CNC content of 5 wt%, whereas a higher CNC content seems to decrease these properties. For the nanocomposites with low degree of crosslinking the Young´s modulus increases from 1.8±0.3 MPa for the neat PMS to 6±0.7 MPa for the PMS/10% CNC nanocomposite while the tensile strength grow from 1.2±0.7 to 5.6±0.4 MPa. The nanocomposites with high degree of crosslinking are much stiffer and stronger (up to 20-fold increase). The best balance of mechanical properties is observed for the 5 wt% CNC sample with a Young´s modulus of 132.5±20.6 MPa, a tensile strength of 20.1±3.4 MPa, and elongation at break of 77±12.6%, and a toughness of 1047±310 MJ/m^3. Interestingly, as can be seen in **Table 2**, the behavior of low content CNCs (1 wt%) nanocomposites for both crosslinking profiles is mainly governed by the PMS matrix, resulting in Young´s modulus and tensile strength values for these nanocomposites close to that of the pure PMS. Moreover, the highly crosslinked nanocomposite with 10 wt% CNCs shows a slightly lower Young´s modulus and a substantially lower elongation at break and toughness that the sample with only 5 wt% CNCs. Given the high hydroxyl functionality of CNCs, which offer an abundance of hydroxyl groups, and considering that the PMS network is established through the formation of ester groups between D-mannitol and sebacic acid, one can surmise that the CNC filler, at least to a certain extent, participates in this reaction through

physical and chemical interactions. As a consequence, the CNCs become part of the PMS network giving more network points through polymer/nanoparticle interactions. This provides higher stiffness without significantly compromising the elongation at break of the composites, which is related to the reinforcement induced by crosslinking reactions between the nanoparticles with high hydroxyl functionality and the matrix, as occur for previously reported polyurethane systems.[52, 53] One must, however, also consider the offset of the stoichiometry between available carboxylic acid and hydroxyl groups. As was mentioned before, the concentration of –OH groups increased from 6, 32 and 62% for 1, 5 and 10 wt% CNC addition respectively (**Table 1, *Supporting Calculation Method M1***). The contribution to the mechanical properties and matrix extensibility of the CNC in the present study could be related to the high –OH groups in the surface of CNC that could strongly interact with the matrix, having a positive effect in the mechanical properties and strain except for high degree of crosslinking nanocomposite and 10 wt% of CNC content. The lowering on the mechanical properties for this sample can probably be ascribed to the high offset in stoichiometry due to the high –OH introduction, also the opposite effect occurs for samples with 1 wt% of CNCs in both crosslinking profiles, the –OH increase is not enough to produce a high enhancement of these properties being the behaviour of these two samples closer than expected to the neat PMS. A high CNC content can presumably induce a shortening of the distance between crosslinking points and thus reducing the flexibility. This would favour the CNC/CNC interactions, reducing the polymer/CNC or polymer/polymer interactions. This situation can hinder the deformation of the system and lower the load transfer between the matrix and the filler because of the loss of polymer/filler synergistic effect.[54] In summary, the higher toughness, the reinforcement effect on mechanical properties, and higher elongation at break for the nanocomposites compared with neat samples, could be related to the

combination of PMS crosslinks and PMS/CNC interactions that attaches the filler to the polymer chains.

DMTA testing. The mechanical properties were further probed as a function of temperature by dynamic mechanical thermal analyses (DMTA). **Figure 4a**, which shows the DMTA traces of samples with a low degree of crosslinking, reveals that in the glassy state the storage modulus (E′) is around 2-3 GPa and is not affected by the introduction of CNCs. Irrespectively of the CNCs content, all the materials with low crosslink density exhibit a glass transition temperature (T_g) of around 18 ºC (as determined with DSC), above which E′ drops to ca. 2-4 MPa; all samples exhibit a rubbery plateau above ca. 40 ºC. The increase in E′ resulting from the introduction of the CNCs is rather modest and is consistent with the observations in other studies based on glassy matrices reinforced with CNCs.[55] For some samples, E′ increases at temperatures between 60-80 ºC, perhaps due to a loss of water or uncured small molecules. **Figure 4b** shows the DMTA traces of the corresponding samples with a high degree of crosslinking. Qualitatively, the curves mirror those of the materials cured under low crosslinking conditions. In the glassy state, the storage moduli are virtually identical to those of the materials described above. The glass transition temperature, as determined by DSC, is slightly increased to 20-26 ºC and the decrease of E' as the temperature is increased to the rubbery plateau is less pronounced. Furthermore, the reinforcing effect induced by the CNC appears to be more significant. For example at 90 ºC E′ is increased from 13 MPa for the neat PMS matrix to 40 MPa for the nanocomposite with 10 wt% CNCs. **Supporting Figure S7** evidences the presence of two maxima in the tangent delta curves, located between 30-40 °C and 50-70 °C, respectively. The temperature of the first maximum coincides with the T_g established by DSC and is assigned to the glass transition. The second tangent delta peak at higher temperatures could be associated

with a restriction in the thermal relaxation of a specific part of the polymeric matrix, indicating the presence of different regions inside of the network. These different domains seem to be induced with high content of CNCs or by combination of CNCs and higher crosslinking density, and can be caused by reactions between CNCs and PMS matrix. As was suggested in mechanical test results, is well known that CNC is highly –OH functional and then, capable to interact with the matrix taking profit of the residual hydroxyl or acid groups from PMS. Thus, it results logical that CNC can have affinity with D-mannitol and sebacic acid, generating a substantial part of the matrix that is forming new physical or chemical interactions with the CNC surfaces, increasing the effective filler-matrix and filler-filler interactions and generating differences in the thermo-mechanical behaviour of these domains not accompanied by a step-wise reduction of E´.

Thermally activated shape-memory properties. The shape-memory properties of the new materials were quantified by cyclic thermomechanical tests conducted in a DMTA, quantifying shape recovery (R_r) and shape fixity (R_f) ratios for each cycle. Initially, a temporary shape was programmed at 45 ºC ($T_{high}>T_g$ determined from the maximum of the tangent delta curves recorded by DMTA) where a stress was applied to elongate the samples to a strain of 30% (Step 1). The samples were subsequently cooled to 15 ºC ($T_{low}<T_g$, tangent delta peak) under a constant stress to fix the programmed temporary shape (Step 2). The load was subsequently removed, the fixity of the temporary shape was quantified at this stress free state (Step 3) and the samples were heated again to 45 ºC (T_{high}) to trigger the thermal recovery of the initial shape (Step 4). As was detailed in the experimental section, samples with high degree of crosslinking were also cycled between 15 ºC (T_{low}) and 60 ºC (T_{high}) as at this temperature all of these nanocomposites are above the upper end of the glass transition (tangent delta peak). **Figure 5** shows exemplarily the shape-memory cycles thus measured for nanocomposites with low

(**Figure 5a**) and high (**Figure 5b**) degree of crosslinking with a CNC content of 5 wt% at programming temperatures of 45 ºC and 60 ºC respectively. **Figure 5a** show a lack of shape memory behaviour for 5 wt% CNC nanocomposite with low degree of crosslinking as these sample is not able to fix the deformed shape at T_{low} after unloading. Under the conditions chosen for the shape memory test, all the samples with low degree of crosslinking have an incomplete shape fixation (R_f<50%) of the programmed shape after cooling and releasing the applied stress, presumably due to the proximity of the fixing temperature (T_{low}) to the T_g (15-23 ºC) as was evidenced in the previous DMTA analysis. By contrast, all samples prepared under high degree of crosslinking conditions showed a shape memory effect with shape fixity R_f >90% after unloading at T_{low}, on account of their higher T_g (**Figure 5b, Supporting Figure S8**). **Figures 6a** and **6b** summarize the shape fixity (R_f) and shape recovery (R_r) values for nanocomposites prepared under high degree of crosslinking conditions tested at recovery temperature of 45ºC. For these samples, the shape fixity remained constant and was close to unity (R_f = 93-96%) without appreciable influence of the CNC content or the number of cycles (**Figure 6a**). In case of the shape recovery for the first cycle (**Figure 6b**) there is a loss in R_r% with increasing CNC content. Neat PMS and 1 wt % CNC sample achieve a R_r of 78% while for 5 and 10 wt % CNC nanocomposites the R_r% decrease to 62%. According to DMTA results, these lower R_r values for the first cycle in nanocomposites with high CNC load can probably be ascribed to the limited movement of the polymer chains due to interactions with CNC.[56] An increased CNC content strongly decreases the magnitude of the transition associated with first delta tangent peak indicating that less mobile units at the recovery temperature of 45 ºC were participating in the relaxation processes resulting in higher non-reversible deformation for 5 and 10 wt% CNC samples during the first cycle (hysteresis). However, in the second cycle the R_r% becomes

significantly higher and stabilizes at values of 99% in the 3rd and 4th cycles. Nevertheless, **Figure 6c** shows how increasing the temperature of the test to 60 ºC allows the samples with 5 and 10 wt% of CNC to achieve R_r% values for the first cycle close to the neat PMS being 100% after the first cycle. At this higher temperature part of the chains associated with the second delta transition have higher mobility evidencing a temperature dependant shape recovery process.[57] However, neat PMS and nanocomposite with 1 wt% of CNC were not able to be cycled at 60 ºC, apparently, due to the lower stiffness of these samples at this temperature that produces premature break **(Supporting Figure S8).** As was explained before, for biomedical uses is of special interest the recovery force that is related with the ability of the material to ensure good shape stability and a complete recovery under restricted environments. **Figure 7** shows that the maximum stress achieved in the shape memory test increased with increasing CNC content. These indicate that the 5 and 10 wt% CNC nanocomposites are able to support a much higher stress, which is concomitant with a higher shape recovery force.[58] This is in agreement with the increase in the Young´s Modulus and rubbery modulus (E´) observed in the mechanical and DMTA tests respectively for these samples. Finally, shape memory effect was obtained for all the highly crosslinked samples at programming temperature of 45 ºC with R_r and R_f close to 100% after the first thermomechanical cycle and no deterioration over the rest of the cycles performed was observed, suggesting good cyclic behaviour. Samples with 5 and 10 wt% CNC also have good shape memory abilities at 60 ºC demonstrating the temperature dependence of the recovery process.

Conclusions

Poly(mannitol-sebacate) pre-polymers with different CNC wt% were prepared using the solution casting method followed by a thermal crosslinking procedure under low and high temperature-time conditions to obtain PMS/CNC nanocomposites with low and high stiffness. For the neat matrix, experimental results demonstrated the possibility to tailor the mechanical properties conform to specific soft or stiff applications depending on the time-temperature curing profiles. In nanocomposites, CNCs introduced high quantity of new hydroxyl groups that could efficiently interact with the matrix increasing the modulus and enhancing the strain and toughness of nanocomposites as compared to the neat polymer matrix probably due to the high filler-matrix compatibility. Nanocomposites with thermally actuated shape memory properties could be achieve for all the samples with high degree of crosslinking at temperatures between 15-45 ºC with R_r and R_f values close to 100% for the second thermo-mechanical cycle. Additionally reduced hysteresis between the first and second cycle could be achieved in highly crosslinked nanocomposites with 5 and 10 wt% of CNC when the temperature of deformation and recovery is 60 ºC without compromising the R_f values having a behaviour similar to the neat matrix. The higher mechanical properties and elongation at break together with the possibility of achieving shape memory properties in the range of physiological temperatures for the nanocomposites with high degree of crosslinking will allow the application of these materials in the biomedical field.

Associated content

Supporting Information

Methods and results of crystallinity, conductometric titration, TEM, ^{1}H-NMR, IR, TGA and DSC studies are shown.

Acknowledgements

The authors gratefully acknowledge financial support received from Spanish Ministry of Economy and Competitiveness (Project MAT2010/21494-C03), as well as the support of FPU grant from MED (MED-FPU; AP2009-2482), Swiss National Science foundation (National Research Programme 64, Project #406440_131264/1) and the Adolphe Merkle Foundation.

References

1. J. P. Bruggeman, B. de Bruin, C. J. Bettinger, R. Langer, *Biomaterials* **2008**, *29*, 4726-4735.

2. Y. Li, G. A. Thouas, Q. Chen, *RSC Adv.* **2012**, 2, 8229-8242.

3. J. Yang, A. Webb, S. Pickerill, G. Hageman, G. Ameer, *Biomaterials* **2006**, *27*, 1889-1898.

4. J. Yang, A. Webb, G. Ameer, *Adv. Mater.* **2004**, *16*, 511-516.

5. H. Park, J. Seo, H. Lee, H. Kim, I. B. Wall, M. Gong, J. C. Knowles, *Acta. Biomater.* **2012**, *8*, 2911-2918.

6. Z. Sun, L. Wu, X. Lu, Z. Meng, Y. Zheng, D. Dong, *Appl. Surf. Sci.* **2008**, *255*, 350-352.

7. Q. Liu, T. Tan, J. Weng, L. Zhang, *Biomed. Mater.* **2009**, DOI: 10.1088/1748-6041/4/2/025015

8. C. Sundback, J. Shyu, Y. Wang, W. Faquin, R. Langer, J. Vacanti, T. Hadlock, *Biomaterials* **2005**, *26*, 5454-5464.

9. Z. Sun, C. Chen, M. Sun, C. Ai, X. Lu, Y. Zheng, B. Yang, D. Dong, *Biomaterials,* **2009**, *30*, 5209-5214.

10. A. Mahdavi, L. Ferreira, C. Sundback, J. W. Nichol, E. P. Chan, D. J. D. Carter, C. J. Bettinger, S. Patanavanich, L. Chignozha, E. Ben-Joseph, A. Galakatos, H. Pryor, I. Pomerantseva, P. T. Masiakos, W. Faquin, A. Zumbuehl, S. Hong, J. Borenstein, J. Vacanti, R. Langer, J. M. Karp, *Proc. Natl. Acad. Sci. U.S.A.* **2008**, *105*, 2307-2312.

11. D. Motlagh, J. Yang, K. Lui, A. Webb, G. Ameer, *Biomaterials* **2006**, *27*, 4315-4324.

12. Y. Wang, G. Ameer, B. Sheppard, R. Langer, *Nat. Biotechnol.* **2002**, *20*, 602-606.

13. I. H. Jaafar, M. M. Ammar, S. S. Jedlicka, R. A. Pearson, J. P. Coulter, *J. Mater. Sci.* **2010**, *45*, 2525-2529.

14. Q. Chen, A. Bismarck, U. Hansen, S. Junaid, M. Q. Tran, S. E. Harding, N. N. Ali, A. R. Boccaccini, *Biomaterials* **2008**, *29*, 47-57.

15. S. Liang, W. D. Cook, G. A. Thouas, Q. Chen, *Biomaterials* **2010**, *31*, 8516-8529.

16. M. A. Meyers, P.Y. Chen, A. Y.M. Lin, Y. Seki, *Prog. Mater. Sci.* **2008**, *53*, 1-206.

17. V. R. Sastri, In Plastics in Medical Devices; Sastri,V. R., Eds.; William Andrew Publishing: Boston, 2010; Chapter 9, pp 217-262.

18. Q. Chen, S. Liang, J. Wang, G. P. Simon, *J. Mech. Behav. Biomed. Mater.* **2011**, *4*, 1805-1818.

19. Q. Liu, J. Wu, T. Tan, L. Zhang, D. Chen, W. Tian, *Polym. Degrad. Stab.* **2009**, *94*, 1427-1435.

20. Q. Chen, L. Jin, W. D. Cook, D. Mohn, E. L. Lagerqvist, D. A. Elliott, J. M. Haynes, N. Boyd, W. J. Stark, C. W. Pouton, E. G. Stanley, A. G. Elefanty, *Soft Matter.* **2010**, *6*, 4715-4726.

21. S. J. Eichhorn, A. Dufresne, M. Aranguren, N. E. Marcovich, J. R. Capadona, S. J. Rowan, C. Weder, W. Thielemans, M. Roman, S. Renneckar, W. Gindl, S. Veigel, J. Keckes, H. Yano, K. Abe, M. Nogi, A. N. Nakagaito, A. Mangalam, J. Simonsen, A. S. Benight, A. Bismarck, L. A. Berglund, T. Peijs, *J. Mater. Sci.* **2010**, *45*, 1-33.

22. M. J. D. Clift, E. J. Foster, D. Vanhecke, D. Studer, P. Wick, P. Gehr, B. Rothen-Rutishauser, C. Weder, *Biomacromolecules* **2011**, *12*, 3666-3673.

23. J. Mendez, P. K. Annamalai, S. J. Eichhorn, R. Rusli, S. J. Rowan, E. J. Foster, C. Weder, *Macromolecules* **2011**, *44*, 6827-6835.

24. L. Hsu, C. Weder, S. J. Rowan, *J.Mater.Chem.* **2011**, *21*, 2812-2822.

25. M. Samir, F. Alloin, J. Sanchez, A. Dufresne, *Macromolecules* **2004**, *37*, 4839-4844.

26. L. Goetz, M. Foston, A. P. Mathew, K. Oksman, A. J. Ragauskas, *Biomacromolecules* **2010**, *11*, 2660-2666.

27. R. Rusli, S. J. Eichhorn, *Appl. Phys. Lett.* **2008**, DOI:10.1063/1.2963491.

28. A. Sturcova, G. Davies, S. Eichhorn, *Biomacromolecules* **2005**, *6*, 1055-1061.

29. A. Lima, J. Wong, M. Paillet, R. Borsali, R. Pecora, *Langmuir* **2003**, *19*, 24-29.

30. C. C. Sun, *J. Pharm. Sci.* **2005**, *94*, 2132-2134.

31. T. Kokubo, H. Kim, M. Kawashita, *Biomaterials* **2003**, *24*, 2161-2175.

32. M. Bellantone, H. Williams, L. Hench, *Antimicrob. Agents Chemother.* **2002**, *46*, 1940-1945.

33. B. Lecouvet, J. Horion, C. D'Haese, C. Bailly, B. Nysten, *Nanotechnology* **2013**, DOI: 10.1088/0957-4484/24/10/105704.

34. K. Prashantha, M. F. Lacrampe, P. Krawczak, *Express Polym. Lett.* **2011**, *5*, 295-307.

35. B. Yakobson, P. Avouris, *Carbon Nanotubes* **2001**, *80*, 287-327.

36. Q. Lu, G. Keskar, R. Ciocan, R. Rao, R. B. Mathur, A. M. R. Rao, L. L. Larcom, *J. Phys. Chem. B* **2006**, *110*, 24371-24376.

37. D. J. Gardner, G. S. Oporto, R. Mills, M. A. S. A. Samir, *J. Adhes. Sci. Technol.* **2008**, *22*, 545-567.

38. H. Koerner, G. Price, N. Pearce, M. Alexander, R. Vaia, *Nat. Mater.* **2004**, *3*, 115-120.

39. J. R. Capadona, O. Van Den Berg, L. A. Capadona, M. Schroeter, S. J. Rowan, D. J. Tyler, C. Weder, *Nat. Nanotechnol.* **2007**, *2*, 765-769.

40. X. Dong, T. Kimura, J. Revol, D. Gray, *Langmuir* **1996**, *12*, 2076-2082.

41. B. Braun, J. R. Dorgan, *Biomacromolecules* **2009**, *10*, 334-341.

42. S. Camarero Espinosa, T. Kuhnt, E. J. Foster, C. Weder, *Biomacromolecules* **2013**, *14*, 1223-1230.

43. E. Lecam, D. Frechon, M. Barray, A. Fourcade, E. Delain, *Proc. Natl. Acad. Sci. U.S.A.* **1994**, *91*, 11816-11820.

44. M. Behl, A. Lendlein, *Mater. Today*, **2007**, *10*, 20-28.

45. W. Wagermaier, K. Kratz, M. Heuchel, A. Lendlein, *Adv. Polym. Sci.* **2010**, *226*, 97-145.

46. D. Ratna, J. Karger-Kocsis, *J. Mater. Sci.* **2008**, *43*, 254-269.

47. C. M. Yakacki, K. Gall, In Shape-Memory Polymers; Yakacki, C.M.; Gall, K., Eds.; Springer-Verlag: Berlin, 2010; Vol 226, pp 147-175.

48. R. Maliger, P. J. Halley, J. J. Cooper-White, *J. Appl. Polym. Sci.* **2013**, *127*, 3980-3986.

49. Q. Chen, In Biomedical Materials and Diagnostic Devices; Qizhi, C., Eds.; Scrivener-Wiley, Beverly, MA, USA, 2012; Chapter 18, pp 529-560.

50. I. Filpponen, D. S. Argyropoulos. *Ind. Eng. Chem. Res.* **2008**, *47*, 8906-8910.

51. A. Patel, A. K. Gaharwar, G. Iviglia, H. Zhang, S. Mukundan, S. M. Mihaila, D. Demarchi, A. Khademhosseini, *Biomaterials* **2013**, *34*, 3970-3983.

52. A. Pei, J. Malho, J. Ruokolainen, Q. Zhou, L. A. Berglund, *Macromolecules* **2011**, *44*, 4422-4427.

53. Y. Tien, K. Wei, *Macromolecules* **2001**, *34*, 9045-9052.

54. M. A. Hood, C. S. Gold, F. L. Beyer, J. M. Sands, C. Y. Li, *Polymer* **2013**, *54*, 6510-6515.

55. K. Shanmuganathan, J. R. Capadona, S. J. Rowan, C. Weder, *J. Mater. Chem.* **2010***, 20*, 180-186.

56. S. A. Abdullah, A. Jumahat, N. R. Abdullah, L. Frormann, *Procedia Eng.* **2012***, 41*, 1641-1646.

57. B. A. Nelson, W. P. King, K. Gall, *Appl. Phys. Lett.* **2005***,* DOI: 10.1063/1.1868883.

58. Q. Meng, J. Hu, Y. Zhu, *J. Appl. Polym. Sci.* **2007***, 106*, 837-848.

Figure Captions

Scheme 1. Schematic representation of the general synthesis of the poly(mannitol- sebacate) pre-polymer. Mannitol (1) was polymerized with sebacic acid (2) into poly(mannitol-sebacate) (PMS) (3). ***Note: some degree of branching taking place at late stages of polymerization cannot be excluded*.

Figure 1. FTIR spectra detail of the -OH region (3500-3200 cm^{-1}) and C=O region (1800-1600 cm^{-1}) for low degree of crosslinking **(L)** and high degree of crosslinking **(H)** neat PMS and PMS/CNC nanocomposites.

Figure 2. Transmission electron micrograph **(TEM)** of the PMS nanocomposite containing 10 wt% CNC and with a high degree of crosslinking, stained with 2% aqueous uranyl acetate solution. Note individualized CNCs indicated by the red arrows.

Figure 3. Typical tensile stress versus strain curves measured at room temperature of neat PMS and PMS/CNC nanocomposites with low degree of crosslinking **(a)** and with high degree of crosslinking **(b)**

Figure 4. DMTA curves showing the storage modulus E´ as a function of temperature of neat PMS and PMS/CNC nanocomposites reacted under low degree of crosslinking conditions **(a)** and high degree of crosslinking conditions **(b)**.

Figure 5. Shape-memory stress-strain-temperature curves of 3 consecutive cycles for low degree of crosslinking PMS/5 wt% CNC nanocomposite **(a)**. Shape-memory stress-strain-temperature curves of 4 consecutive cycles for high degree of crosslinking PMS/5 wt% CNC **(b)**.

Figure 6. Shape fixity **(a)** and shape recovery **(b)** characteristic values for the first and second cycles of neat PMS and PMS/CNC nanocomposites with high degree of crosslinking obtained at recovery temperature of 45 ºC. Comparative of the first cycle shape recovery values obtained at two different recovery temperatures (45 ºC and 60 ºC) for 5 and 10 wt% of CNC nanocomposites with high degree of crosslinking **(c)**.

Figure 7. Dependence of maximum stress (σ_{max}) with CNC content for PMS/CNC nanocomposites with high crosslinking degree during the first shape-memory test for 30% of elongation (ε_m).

Table 1

Percentage of OH groups introduced by the CNC addition in the PMS matrix. The total amount of –OHs available on 1g of PMS matrix was estimated assuming an ideal linear pre-polymer with four available –OHs per mannitol molecule taking into account the molecular weight value obtained from GPC experiments. The total amount of –OHs available on the CNC introduced in each sample (1, 5 and 10 wt%) was estimated taking in account the molecular weight of native cellulose with 20% of the total –OHs as reactive sites. As the addition of CNCs slightly changes the volume of the nanocomposites, the amount of moles, were adjusted to molarity taking in account the mass density of the materials obtained using a pycnometer (50 cm^3). Mass densities were obtained from dried pre-PMS and pre-PMS/CNC (1, 5 and 10 wt% of CNC) nanocomposites, previously treated at 120 ºC and 60 cmHg for 1 day to achieve a minimum stiffness and the same treatment for all the samples.

Table 1 Amount of –OH groups introduced by CNC in the Pre-PMS samples

Pre-PMS -OH available (mol) [a]	CNC (wt%)	Cellulose -OH available (mol) [b]	Total -OH available in the sample (mol)	Increase amount of -OH in the sample (%)	ρ (g/cm^3) [c]	-OH molarity (mol/cm^3) [d]
$5.3e^{-4}$	0	0	$5.3e^{-4}$	0	0.70±0.08	0.37
	1	$3.3e^{-5}$	$5.6\ e^{-4}$	6	0.96±0.04	0.54
	5	$1.6e^{-4}$	$6.9\ e^{-4}$	31	1.15±0.03	0.80
	10	$3.2e^{-4}$	$8.6\ e^{-4}$	62	1.16±0.03	1.00

[a] Determined from GPC Pre-PMS M_w, considering 4 reactive –OH per molecule
[b] Determined considering 180.1g/mol as a M_w of cellulose and 20% of reactive –OHs
[c] Samples were maintained 1 day at 120 ºC under 60 cmHg before measuring the density with a pycnometer (50 cm^3)
[d] Determined taking in account the mass densities of the samples

Table 2

Physical and mechanical properties of neat PMS and PMS/CNC nanocomposites (1, 5 and 10 wt% CNCs), prepared under different curing conditions (low (**L**) and high (**H**) degree of crosslinking).

Table 2 Curing conditions, physical and mechanical properties of PMS and nanocomposites

Sample	Crosslinking conditions	Young´s modulus (MPa) [a]	Ultimate tensile strength (MPa) [a]	Elongation at break (%) [a]	Tg by DSC (ºC) [b]	Tg by DMTA (ºC) [c]	Toughness (MJ/m^3) [a]
Neat PMS	Low degree of crosslinking **(L)**; 120ºC, -60cm Hg, 3 days	1.8±0.3	1.2±0.7	80.0±29.0	18	21	63.6±50.0
PMS/1% CNC		2.1±0.5	2.3±0.02	147.0±31.1	18	22	187.4±46.3
PMS/5% CNC		3.0±0.3	4.6±0.6	166.0±20.5	18	23	393.5±5.2
PMS/10%CNC		6.0±0.7	5.6±0.4	119.5±18.3	17	14	389.0±86.4
Neat PMS	High degree of crosslinking **(H)**; **L** + 170ºC, -60cm Hg, 1day	54.4±3.3	7.0±0.6	40.5±7.0	26	34	204.4±6.3
PMS/1% CNC		54.5±1.6	13.2±2.2	94.1±14.0	24	42	757.4±238.0
PMS/5% CNC		132.5±20.6	20.1±3.4	77.0±12.6	21	34	1047.0±310.0
PMS/10%CNC		103.0±12.2	19.4±2.4	37.4±6.0	20	32	470.0±102.2

[a] Determined from stress strain curves

[b] Determined from differential scanning calorimetry traces *(see Supporting Information , **Figure S9**)*

[c] Determined from the delta tangent peak of dynamic mechanical analysis curves

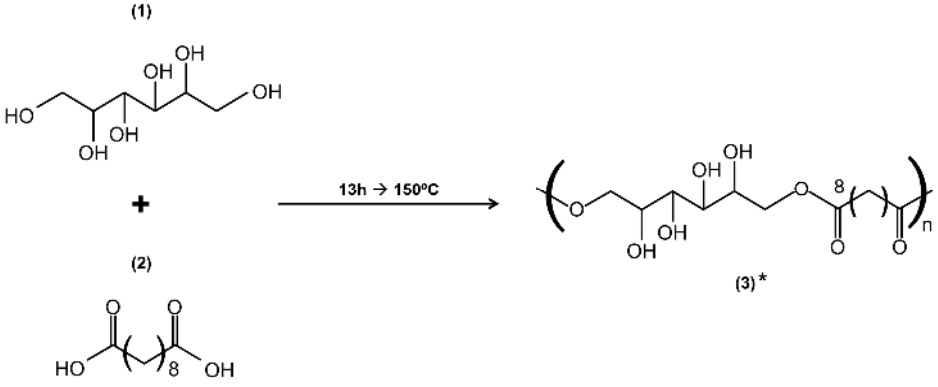

419x178mm (300 x 300 DPI)

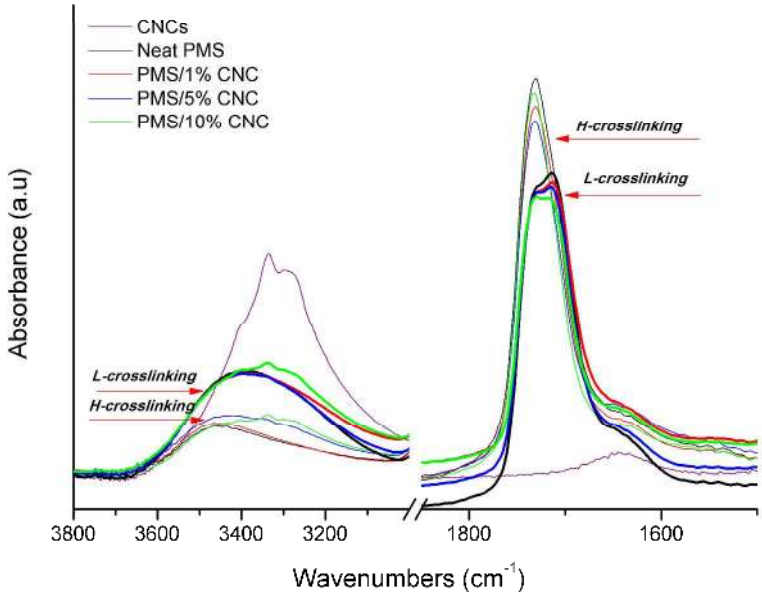

287x201mm (300 x 300 DPI)

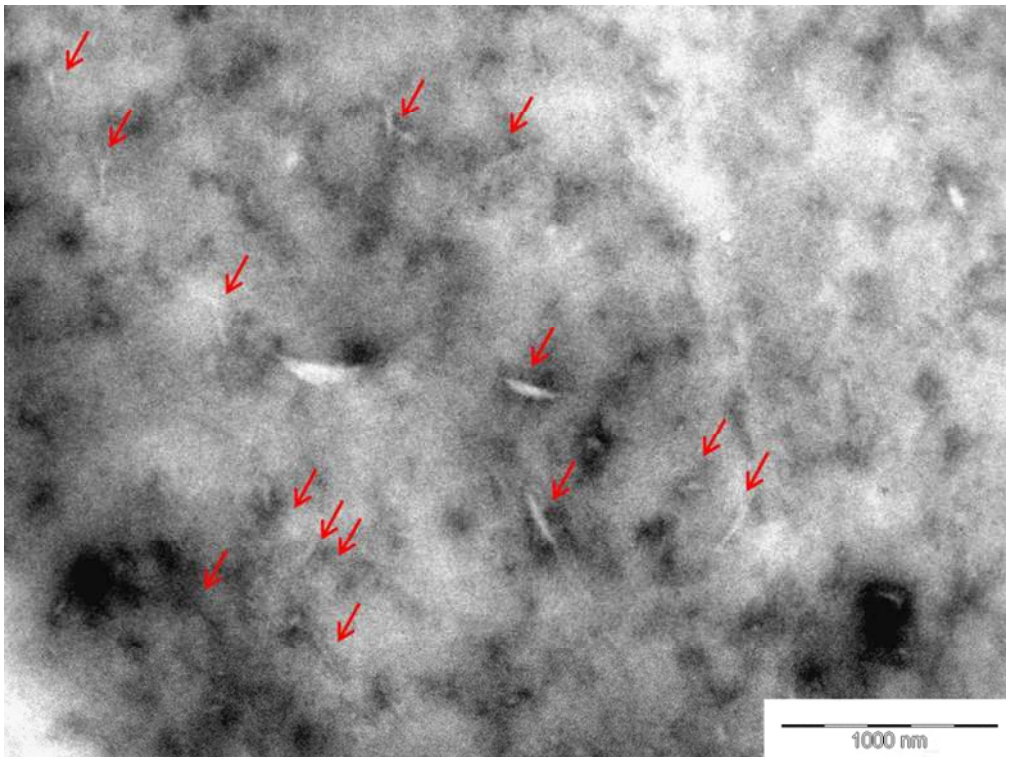

153x114mm (300 x 300 DPI)

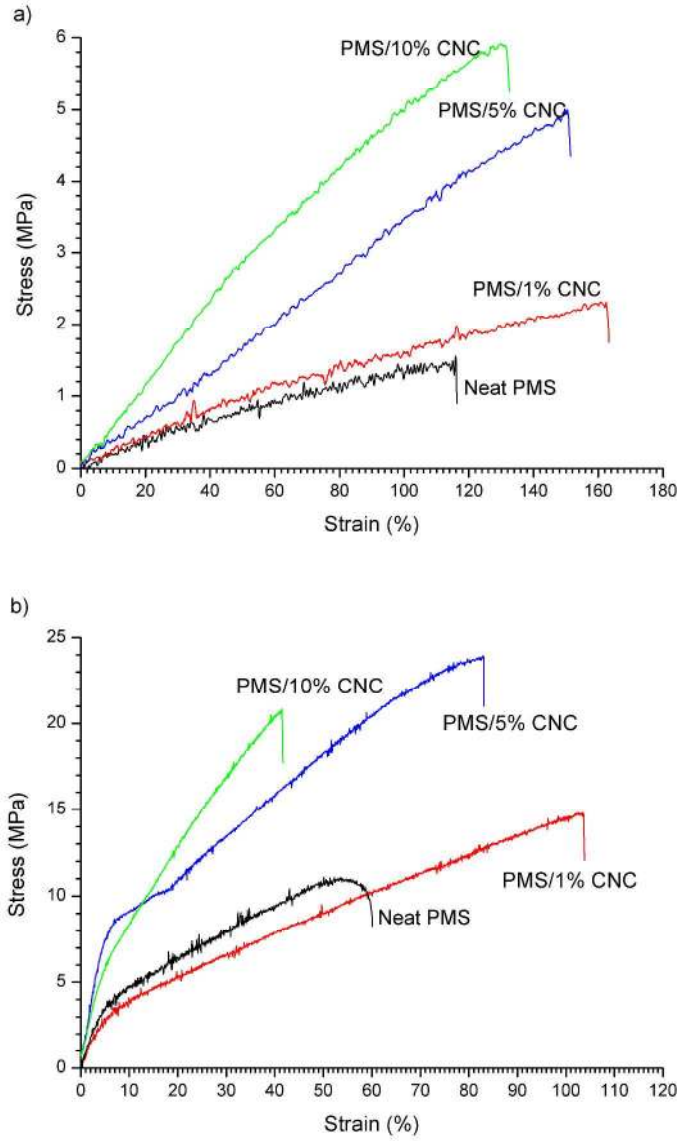

287x403mm (300 x 300 DPI)

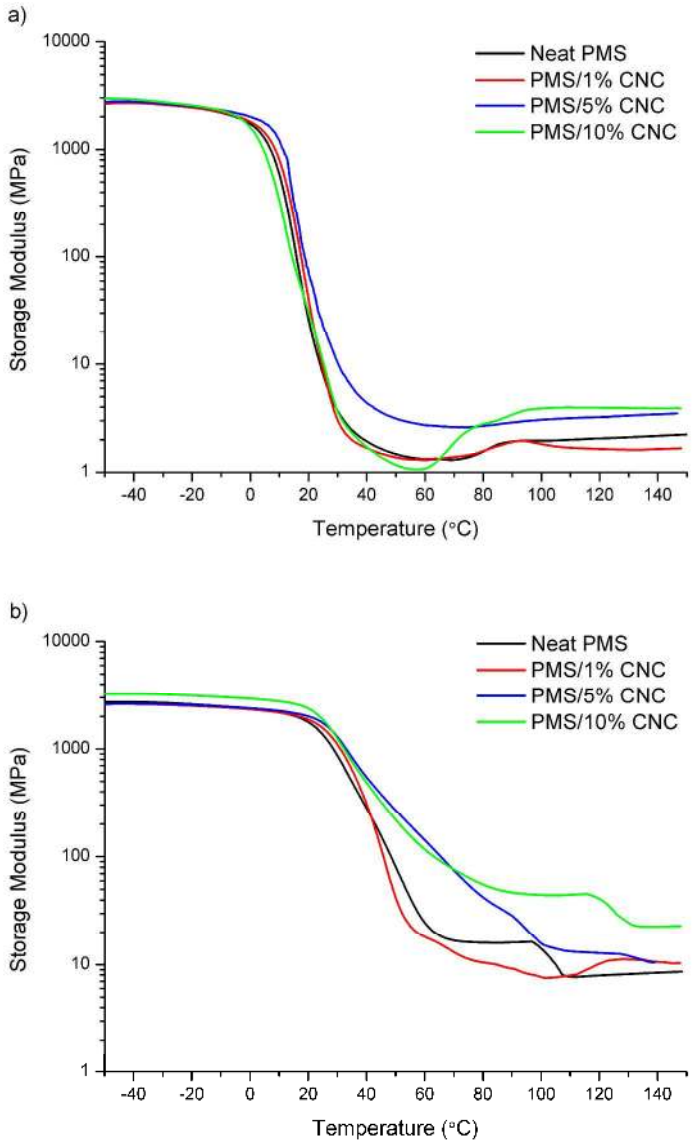

287x403mm (300 x 300 DPI)

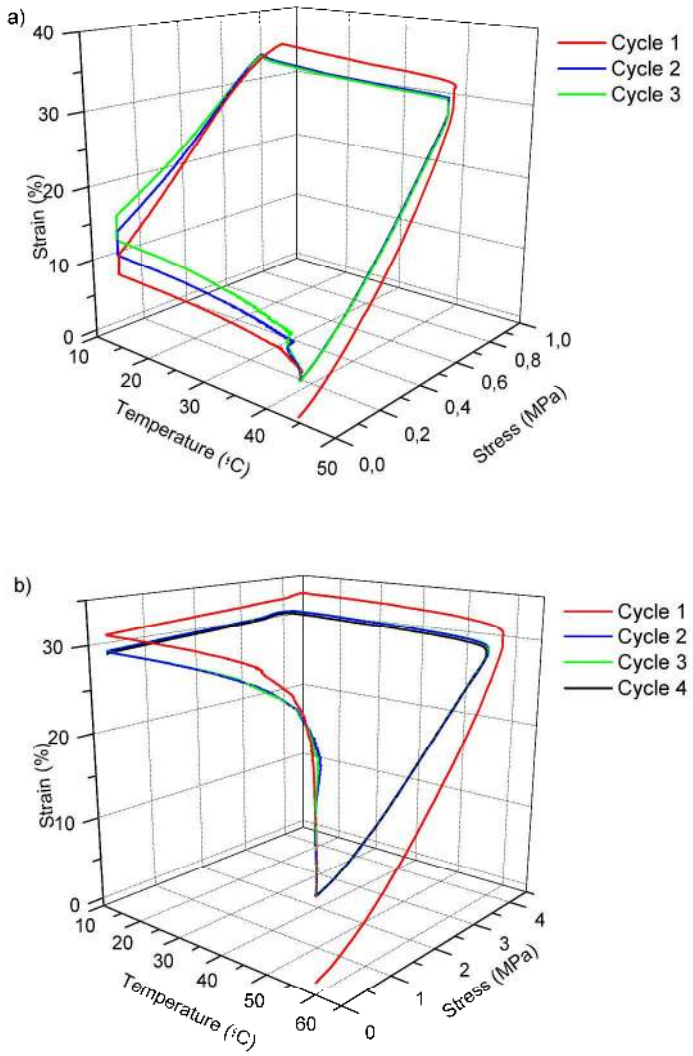

287x415mm (300 x 300 DPI)

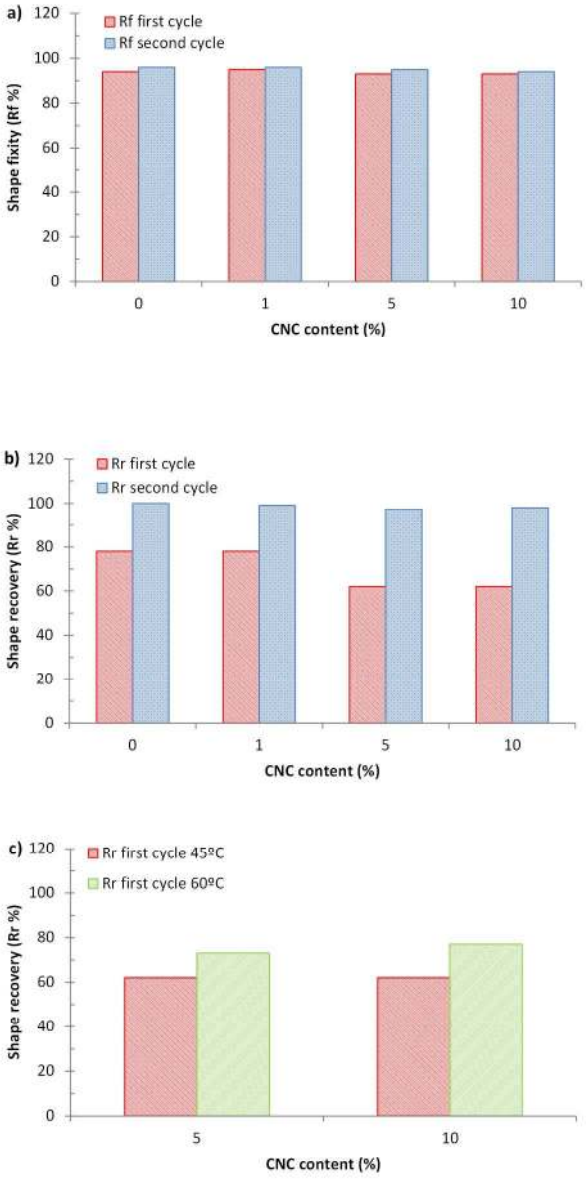

128x248mm (300 x 300 DPI)

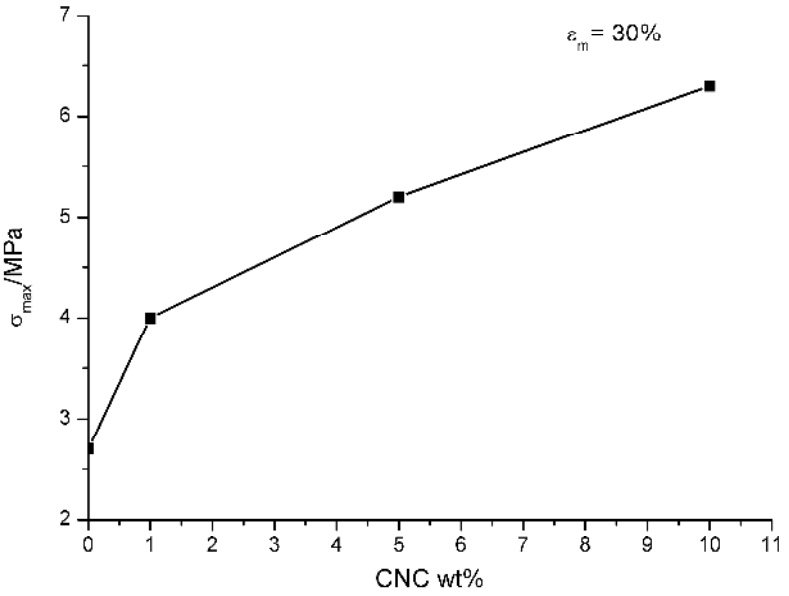

287x201mm (300 x 300 DPI)

Graphical abstract

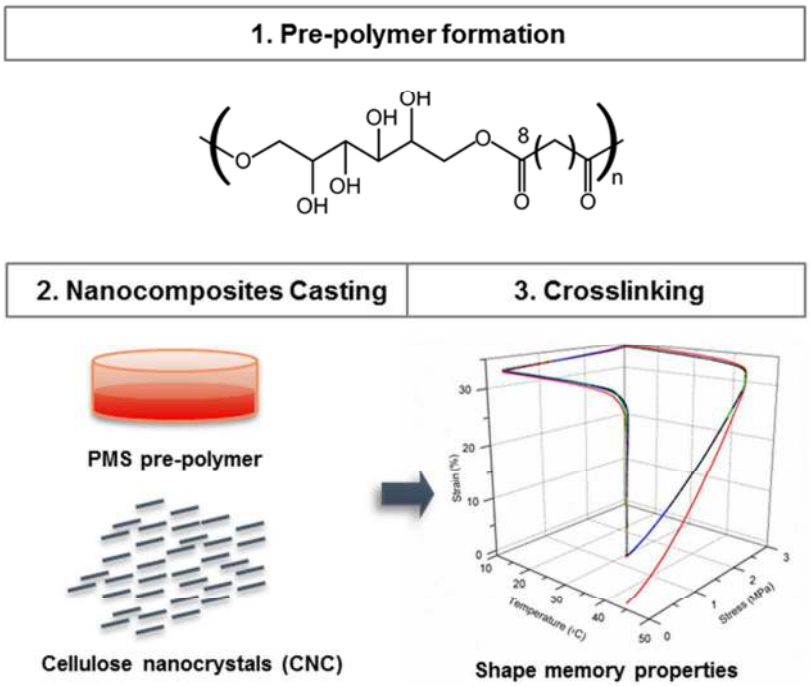

The synthesis of nanocomposites of poly(mannitol-sebacate) (PMS) and cellulose nanocrystals (CNCs) was achieved in two steps. A low-molecular-weight prepolymer that was soluble in common solvents was first formed via the polycondensation reaction between sebacic acid and D-mannitol. Nanocomposites with different CNC contents were subsequently prepared by solution casting and curing under vacuum. The new materials display a shape-memory effect.

Supporting Information

Mechanical and shape-memory properties of poly(mannitol sebacate) / cellulose nanocrystal nanocomposites

Águeda Sonseca[1*], *Sandra Camarero-Espinosa*[2], *Laura Peponi*[3], *Christoph Weder*[2], *E. Johan Foster*[2], *José M. Kenny*[3], *and Enrique Giménez*[1]

[1]Instituto de Tecnología de Materiales, Universidad Politécnica de Valencia (UPV), Camino de Vera s/nº, 46022 Valencia (SPAIN)

[2]Adolphe Merkle Institute, University of Fribourg, Rte de l´Ancienne Papeterie, PO Box 209, CH-1723 Marly (SWITZERLAND)

[3]Instituto de Ciencia y Tecnología de Polímeros (ICTP-CSIC), Juan de la Cierva 3, 28006 Madrid (SPAIN)

Table S1

Composition and molecular weight distribution of PMS pre-polymer after 13 h of polycondensation reaction of sebacic acid and mannitol monomers under continuous stirring and nitrogen flow at 150 ºC.

Table 1. Main PMS Pre-Polymer Properties	
Composition by ^{1}H NMR	1:0.93
M_w (g/mol)[a]	7501
M_n (g/mol)[b]	6180

[a]M_w: weight average molecular weight. [b]M_n: number average molecular weight.

CNC properties.

Charge concentration was determined by conductometric titration (**Figure S4**). Dimensions and aspect ratio of CNCs were calculated as an average of randomly measures in TEM images at different magnifications (2950x, 3900x and 5200x). ImageJ software (National Institute of Health in USA) was used to evaluate the length and width of the CNCs. Apparent crystallinity was calculated from X-ray diffraction pattern (**Figure S3**).

Table S2. Main CNCs properties analysed through conductometric titration, TEM images and X-ray diffraction pattern.

Table S2. Main CNCs Properties

charge concentration ($mM/kg_{cellulose}$)[a]	91 ± 4
length (nm)	199 ± 14
width (nm)	18 ± 2
aspect ratio	11 ± 1
apparent crystallinity (%)	68

[a]Determined by conductimetric titration

Transmission Electron Microscopy of CNCs

CNCs TEM micrographs were recorded in a Phillips CM10 microscope with an accelerating voltage of 80kV. Samples were prepared by drying a drop of dilute whiskers suspension in H_2OD (0.1 mg/mL) onto a carbon-coated copper grid (Electron Microscopy Sciences) and subsequently dried under a lamp for 1 h.

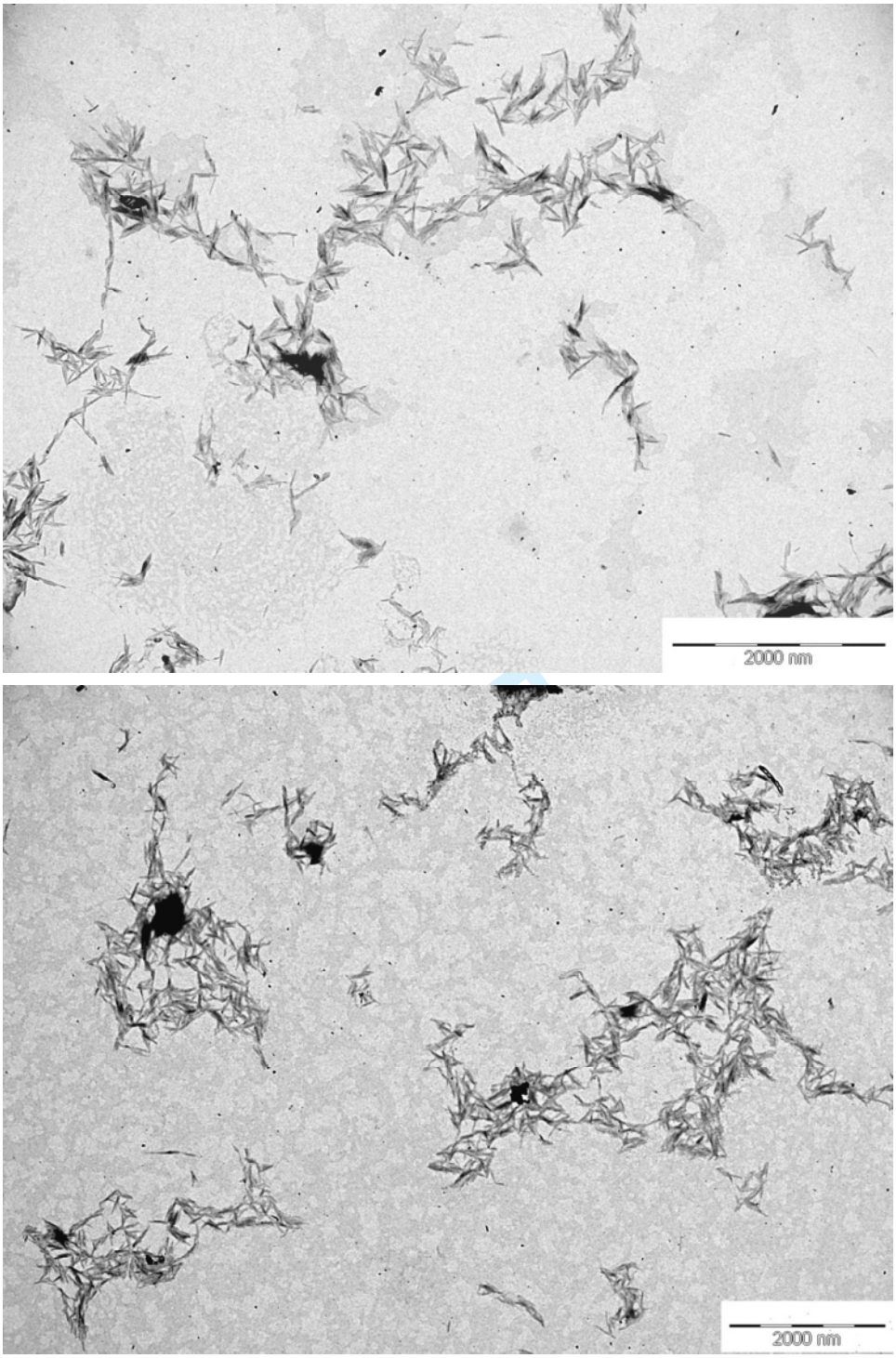

Figures S1 and S2. Transmission electron micrographs (TEM) of CNC isolated by hydrolysis with sulfuric acid.

X-Ray Diffraction (XRD)

The crystalline structure of the CNCs was investigated with an RXSiemens D5000 equipped with a Cu Kα radiation source (λ = 1540 A) operating at 40 kV. A CNC sample was dispersed in water and dried in oven at 100 ºC for 0.5 h. After drying the compact powder obtained was regrounded and transferred to scan. The scanning range was 2º-40º, step-size and count time per step were 0.02º and 8 seconds, respectively. To calculate the apparent crystallinity, difractogram was fitted using www.magicplot.com software. Gaussian shaped peaks were assumed and let free for intensity, position and FWMH after background subtraction, and non-crystalline peak was fixed at position. Data was deconvoluted taking into account only cellulose type I.[1, 2]

(101):14.8º, (10I): 16.7º, (021): 21.7º, (002):22.8º and (040): 34.7º

The percentage of apparent crystallinity was estimated from the ratio of the crystalline area peaks to the total area including the non-crystalline peak (equation 1) to be ~68%.

Equation (1)

$$A.C = 100\ \frac{I_{(101)} + I_{(10I)} + I_{(021)} + I_{(002)} + I_{(040)}}{I_{(101)} + I_{(10I)} + I_{(021)} + I_{(002)} + I_{(non\ crystalline)}}\ [\%]$$

where A.C means apparent crystalinity and $I_{(xxx)}$ is the area under the peak.

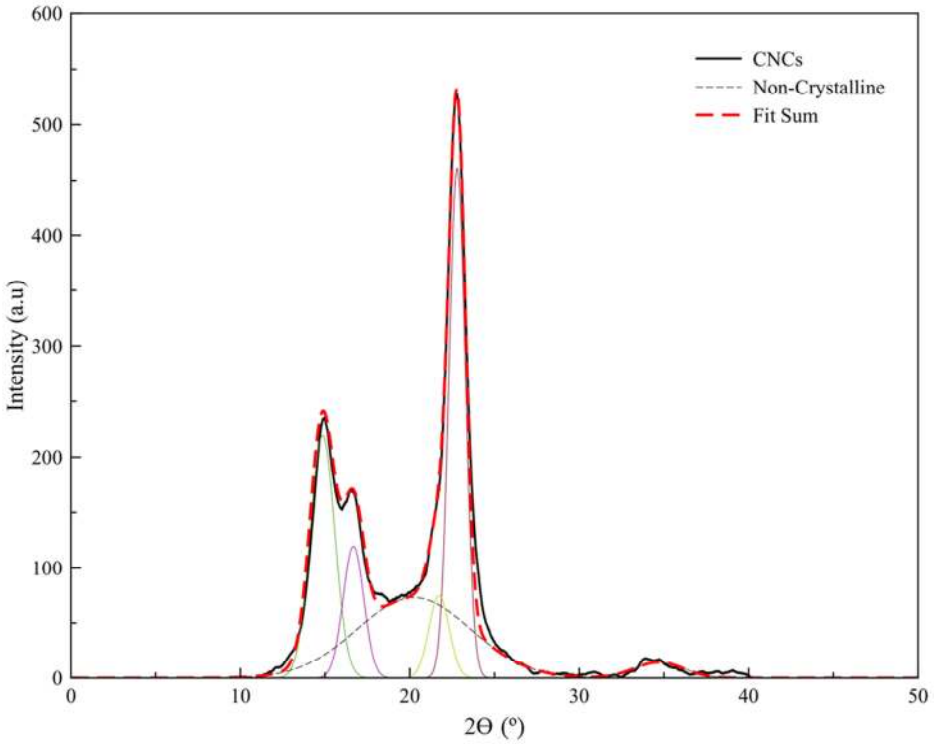

Figure S3. X-Ray diffractogram of CNCs. Data was fitted taking into account crystalline peaks of cellulose type I.

Conductometric titration of CNCs.

To determine the surface charge density, CNCs were conductometric titrated as described previously.[3, 4] Briefly ≈ 50 mg of CNCs were dispersed via sonication in a mixture of 10 mL of 10 mM aqueous hydrochloric acid and 25 mL of ultrapure H_2O. The sample was titrated with aliquots of 10 mM aqueous NaOH recording the conductivity after the addition of each aliquot. The concentration of sulphate groups on CNCs was calculated from the titration results according to a reported protocol.[5]

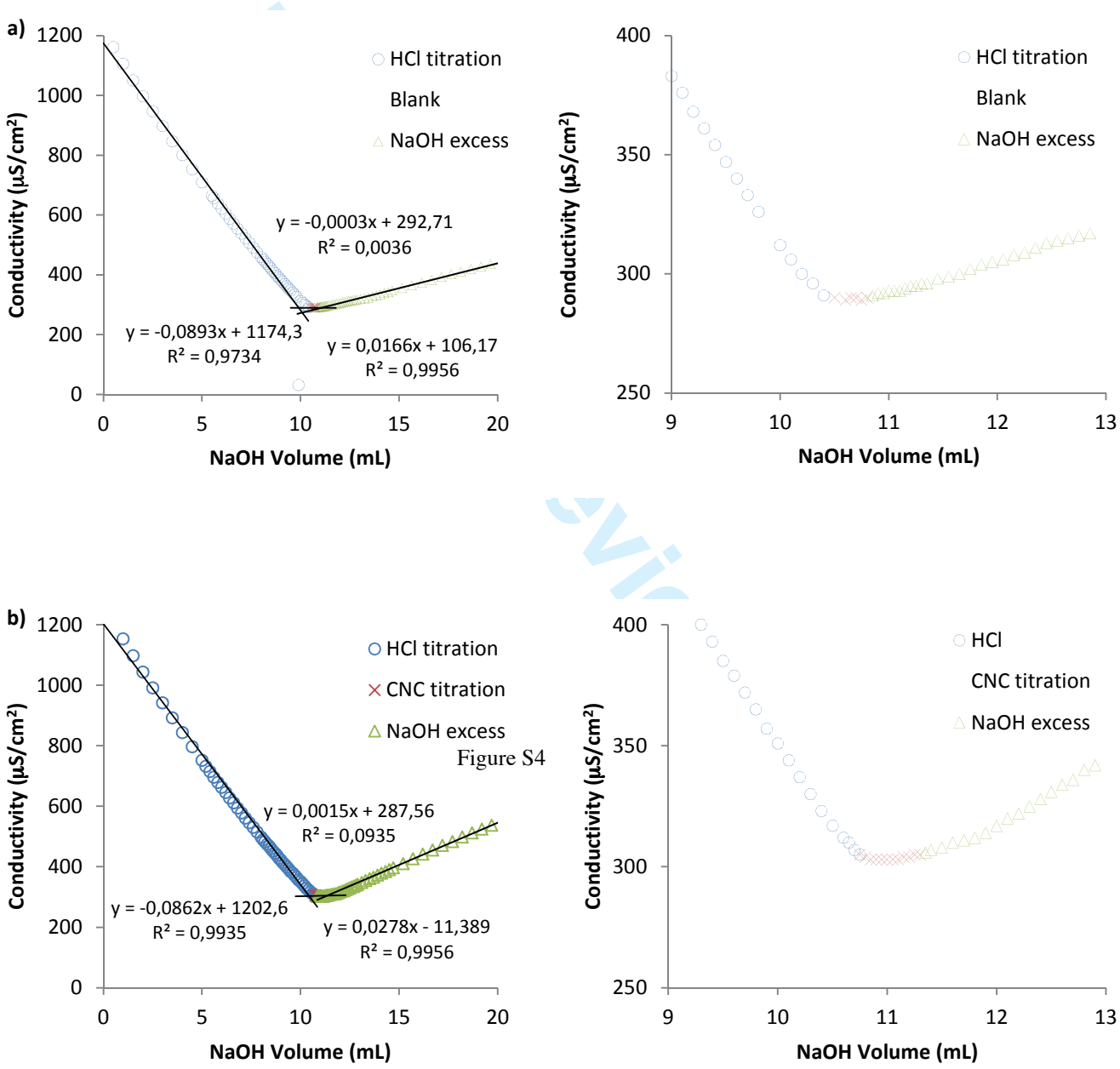

Figure S4

Figure S4. Conductometric titration curves of a) neat medium and b) CNCs

Calculation Method M1. Percentage of OH groups introduced with the CNC addition in the PMS matrix.

The total amount of –OHs available on 1g of PMS matrix was estimated supposing an ideal linear pre-polymer with 4 available OHs per mannitol molecule taking into account the molecular weight value obtained from GPC (7501 g/mol) test.

The quantity of –OHs available in 1g of pre-PMS was calculated following the equation:

$$\left(\frac{W_{pre-PMS}}{Mw_{pre-PMS}}\right) x\ 4 = mol_{available-OH}$$

obtaining a value of ***5.3 e^{-4}*** mol of available -OH in 1g of pre-PMS matrix.

The total amount of –OHs on the CNC was estimated taking in account the molecular weight of native cellulose (180.1 g/mol) and supposing 3 available OHs per cellulose unit. Only the 20% of the total –OHs was considered as reactive sites [6]

The total amount of –OHs available on the CNC introduced in each sample (0.01, 0.05 and 0.1 g for 1, 5 and 10 wt% of CNC samples respectively) was calculated following the equation:

$$\left(\left(\frac{W_{CNC}}{Mw_{CNC}}\right) x\ 3\right) x\ 0.2 = mol_{available-OH}$$

obtaining values of ***3.3 e^{-5}***, ***1.6 e^{-4}***, ***3.3 e^{-4}*** for 1, 5 and 10 wt% of CNC addition in 1g of pre-polymer.

The increase % of –OH per sample was calculated relative to the available OH in the pre-polymer matrix with the following equation:

$$\left(\frac{mol_{available-OH\ in\ CNC}}{mol_{available-OH\ in\ pre-PMS}}\right) x100 = increase\ \%\ of\ -OH\ in\ each\ sample$$

Obtaining an approximate increase of 6, 30 and 60 % of –OHs with 1, 5 and 10 wt% of CNC addition.

[1]H-NMR studies

A [1]H-NMR spectrum of the PMS pre-polymer was obtained in deuterated dimethylsulfoxide (DMSO- d_6) on a Varian Mercury VX-300 MHz NMR spectrometer. The sample was prepared dissolving the prepolymer in 750 μL of d_6DMSO in a glass tube. The peaks from the mannitol appeared at 3.5-5.5 ppm due to central and terminal methylene units identified by hydrogens on the carbons "a" and "b". The protons from the methylene units of sebacic acid showed peaks at 1.3, 1.6 and 2.3 ppm identified by hydrogens on the carbons "c", "d" and "e" respectively. The peak at 3.3 was due to residual water.[7] Note that as the monomers are multifunctional, at late stages of polymerization some degree of branching can take place and cannot be excluded completely.

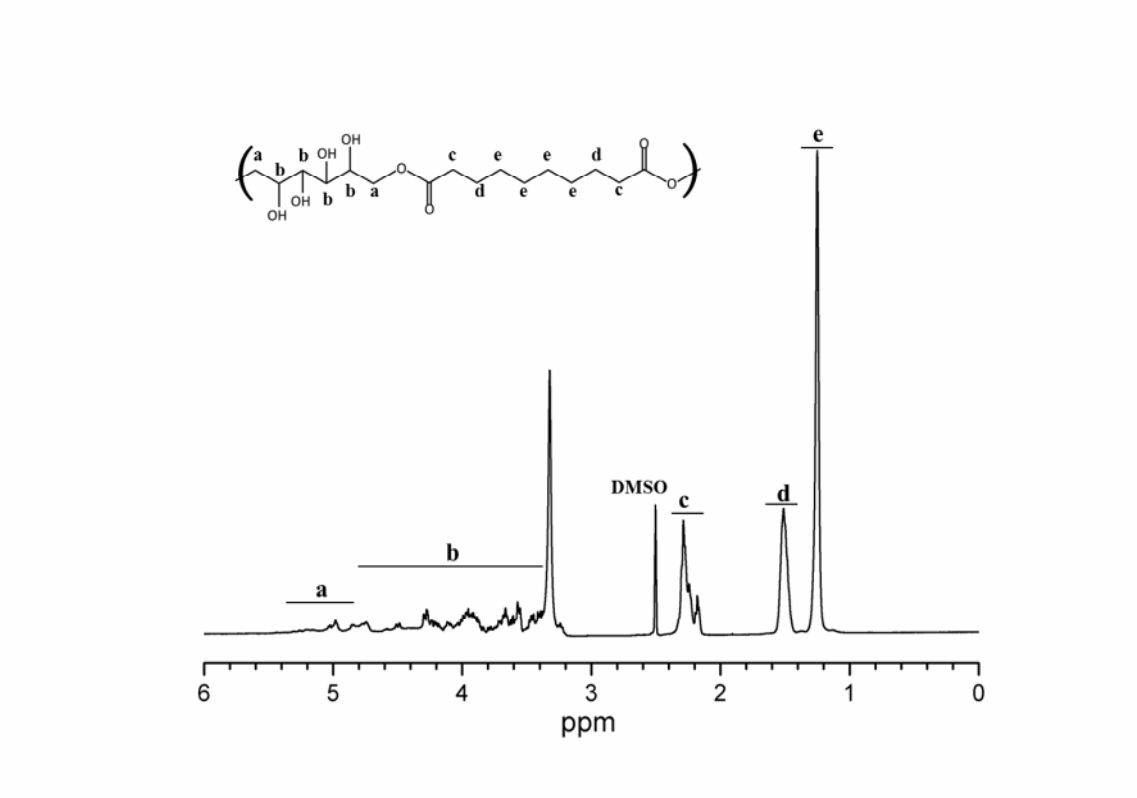

Figure S5. [1]H-NMR spectrum of the PMS pre-polymer, recorded in DMSO- d_6.

Fourier Transform Infrared Spectroscopy (FTIR).

Transmission spectra were recorded using a Thermo Nicolet 5700 spectrometer, in the 500 to 4500 cm^{-1} region, with a 4 cm^{-1} resolution with an Attenuated Total Reflectance (ATR) cell. Backgrounds were acquired before every 3rd sample. All samples were vacuum-dried before measurement.

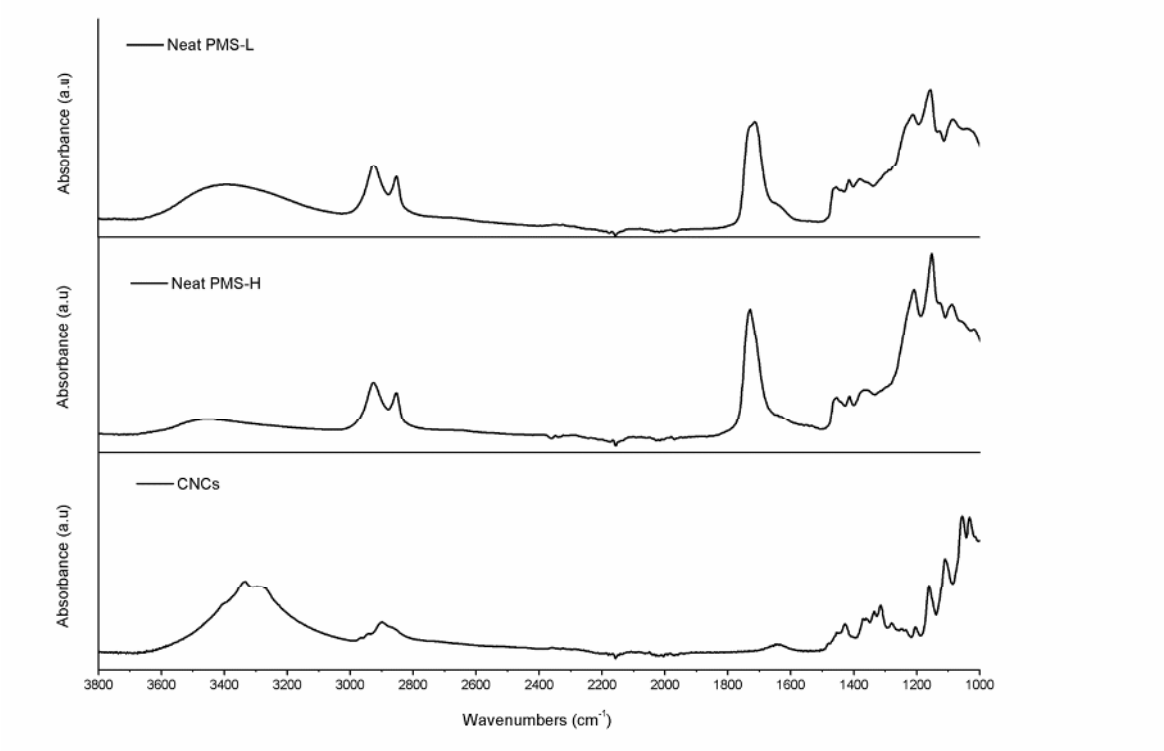

Figure S6. FTIR spectra from top to bottom, neat PMS with low degree of crosslinking **(L)**, high degree of crosslinking **(H)** and CNCs.

Dynamic Mechanical Thermal Analysis (DMTA) tan δ curves

The mechanical behaviour as a function of the temperature was characterized by DMTA measurements in a TA Q800 instrument (TA instruments) in tensile mode with a temperature ramp method from -50 to 150 ºC at a heating rate of 3 ºC/min. Frequency and strain amplitude were kept constant at 1 Hz and 15 μm, respectively.

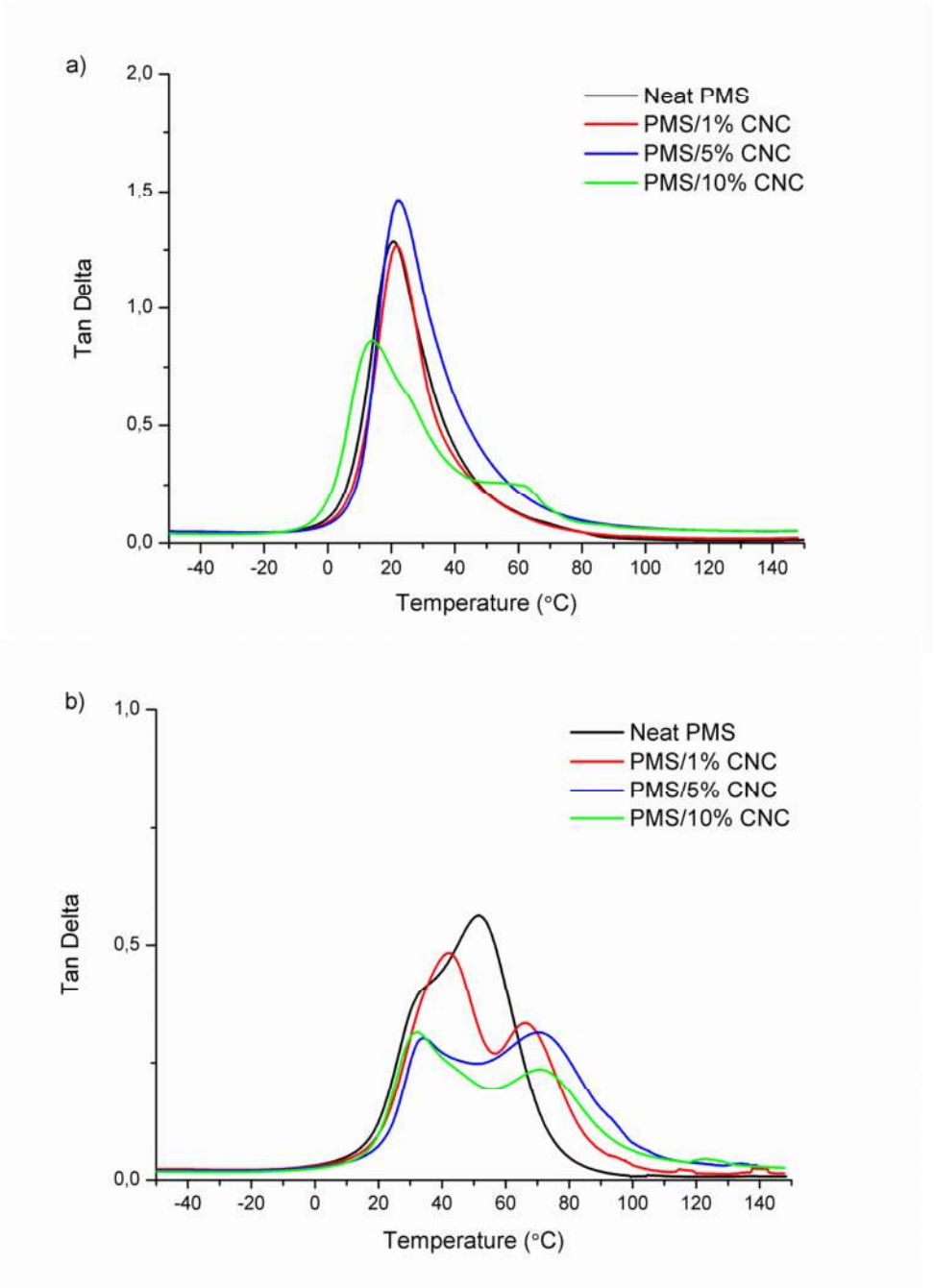

Figure S7. DMTA delta tangent curves as a function of temperature of neat PMS and PMS/CNC nanocomposites reacted under low degree of crosslinking **(a)** and high degree of crosslinking conditions **(b)**.

Thermally activated shape-memory properties

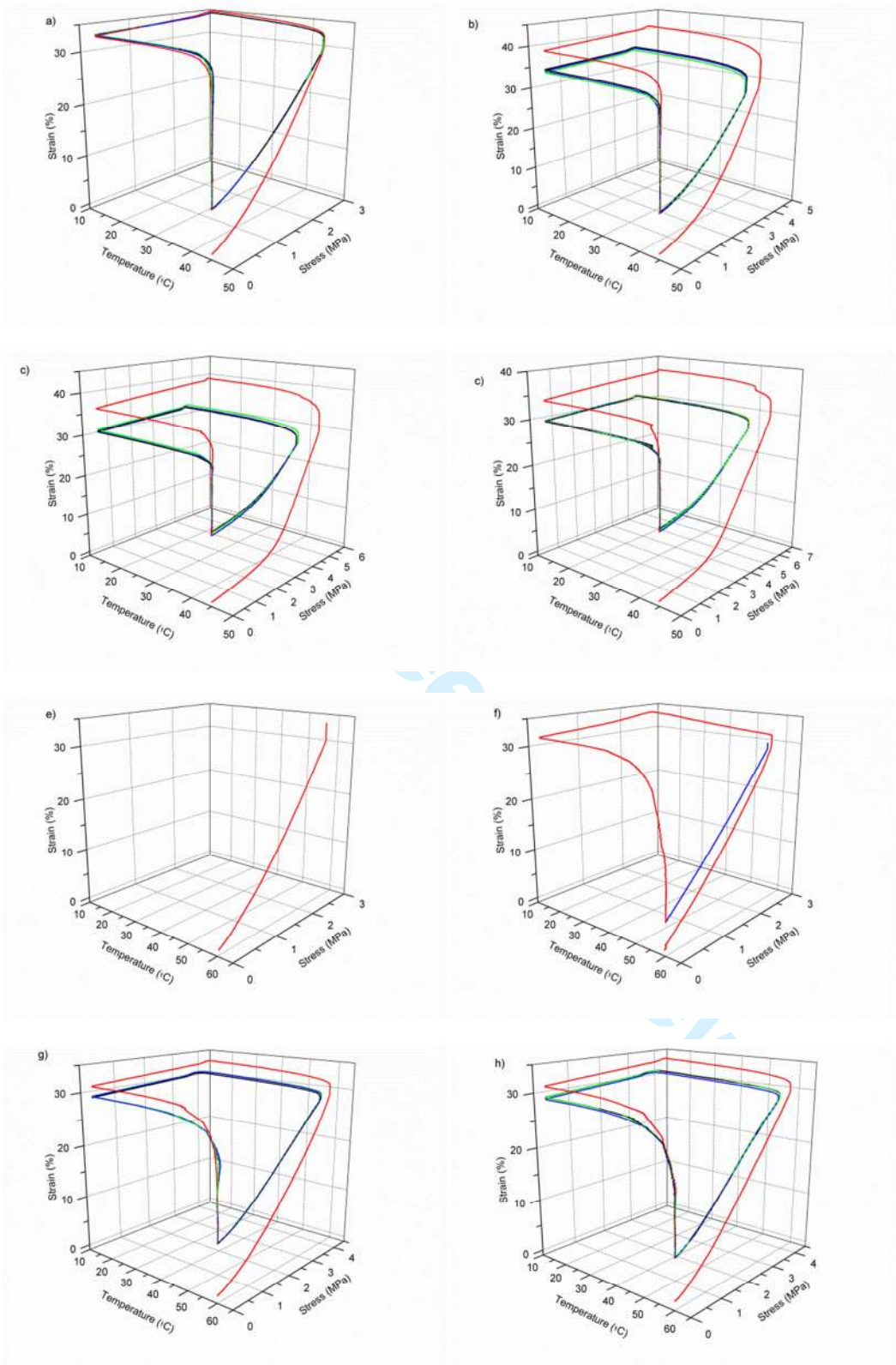

Figure S8. Shape-memory stress-strain-temperature curves of consecutive cycles for high degree of crosslinking PMS and PMS/CNC nanocomposites. Neat PMS **(a)**, 1wt% CNC **(b)**, 5wt% CNC **(c)** and 10

wt% CNC **(d)** with programming-recovery temperature of 45ºC. Neat PMS **(e)**, 1wt% CNC **(f)**, 5wt% CNC **(g)** and 10 wt% CNC **(h)** with programming-recovery temperature of 60 ºC.

Thermo gravimetric Analysis (TGA).

Thermal stability of all the obtained samples and the CNCs was recorded in a Mettler-Toledo TGA/SDTA 851^e modulus analyser. The samples (5-10 mg) were weighted in zircona crucibles and were heated in air at a rate of 10 ºC/min from ambient to 700 ºC. **Figure S8** shows the thermogravimetric profile for all the composites and for CNC. Typically, H_2SO_4-CNC, showed two well separated degradation processes, one started from 220 to 280 ºC (attributed to depolymerisation, dehydration, and decomposition of glycosyl units followed by the formation of a char) and the other was between 330 to 500 ºC (attributed to the oxidation and breakdown of the char to lower molecular weight gaseous products).[8] In case of thermal stability of the films, TGA curves of neat PMS and CNC load samples with high degree of crosslinking revealed an increase of thermal stability for these curing conditions compared with the low degree of crosslinking samples, that is, the initial drop in the slop occurred at higher temperature for samples with high degree of crosslinking. PMS/CNC nanocomposites containing 5-10 wt% of CNC showed slightly lower onset degradation temperature than neat PMS due to the lower onset degradation temperature of CNC than the matrix.

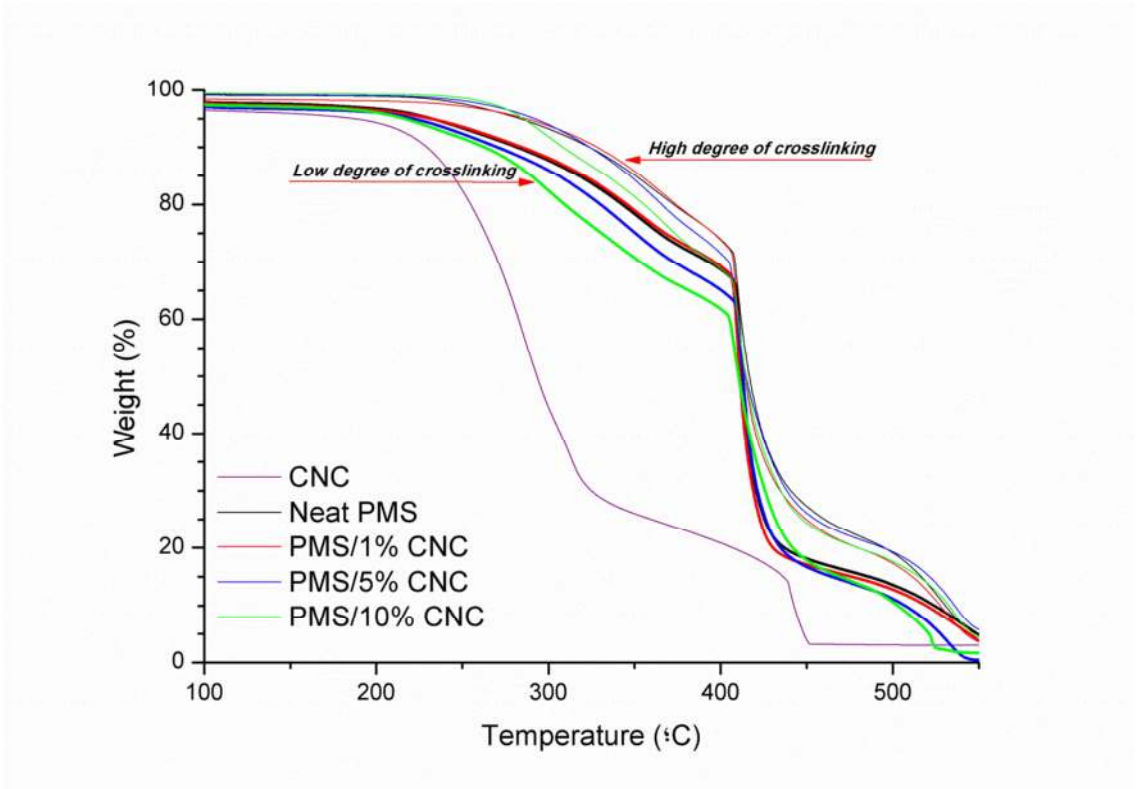

Figure S8. TGA curves of CNC, neat PMS and PMS/CNC nanocomposites with low and high degree of crosslinking.

Differential Scanning Calorimetry (DSC).

Thermal behaviour was studied in a Mettler-Toledo DSC 800 under N_2 atmosphere. Samples were heated from -60 to 180 ºC, cooled down from to -60 ºC and heated up again to 180 ºC at a heating/cooling rate of 10ºC/min under a nitrogen atmosphere. The glass transition temperatures (Tg) were calculated as the midpoint of the transition in the 2nd heating run for all the samples. **Figure S9** shows the differential scanning calorimeter (DSC) second heating run for all the samples. All the high crosslinked samples had a Tg higher than the low crosslinked ones, that is, longer curing times and temperatures derivate in a higher degree of crosslinking. It could be due to the fact that hydrogen bonding and/or chemical crosslink was gradually intensified during thermal curing limitating the mobility of polymeric chains increasing the Tg and also the thermal stability. Generally, nanofillers are expected to increase considerably the Tg of materials difficulting chain motions of the matrices, however, we observed no significant influence of CNC content in the Tg of the low degree of crosslinking samples, and in samples with high degree of crosslinking the Tg tended to decrease while increasing the CNC content. This all phenomena could be explained as follows; in the first step of the condensation, a 1:1 molar ratio of the reactants produced an esterification dominated by the reaction of the primary hydroxyl groups founded at both ends of mannitol with carboxylic acid groups from sebacic acid, leaving a large amount of secondary –OH groups in the prepolymer. CNCs were added into the PMS prepolymer at this point and were sommeted to a curing under vacuum and temperature. CNC changed considerably the OH/COOH ratio due to the higher -OH groups content in the surface of the filler, variating the stoichiometry reaction of the neat PMS samples, increasing ratio of –OH groups and favouring the interactions between CNC and matrix and CNC-CNC being more notable under high crosslinking profile and higher filler loads. These changes in the initial OH/COOH ratio of the monomers seemed to be responsible for CNC was not producing a notable increase in the Tg as was expected or even shifted to lower temperature for nanocomposites.[9]

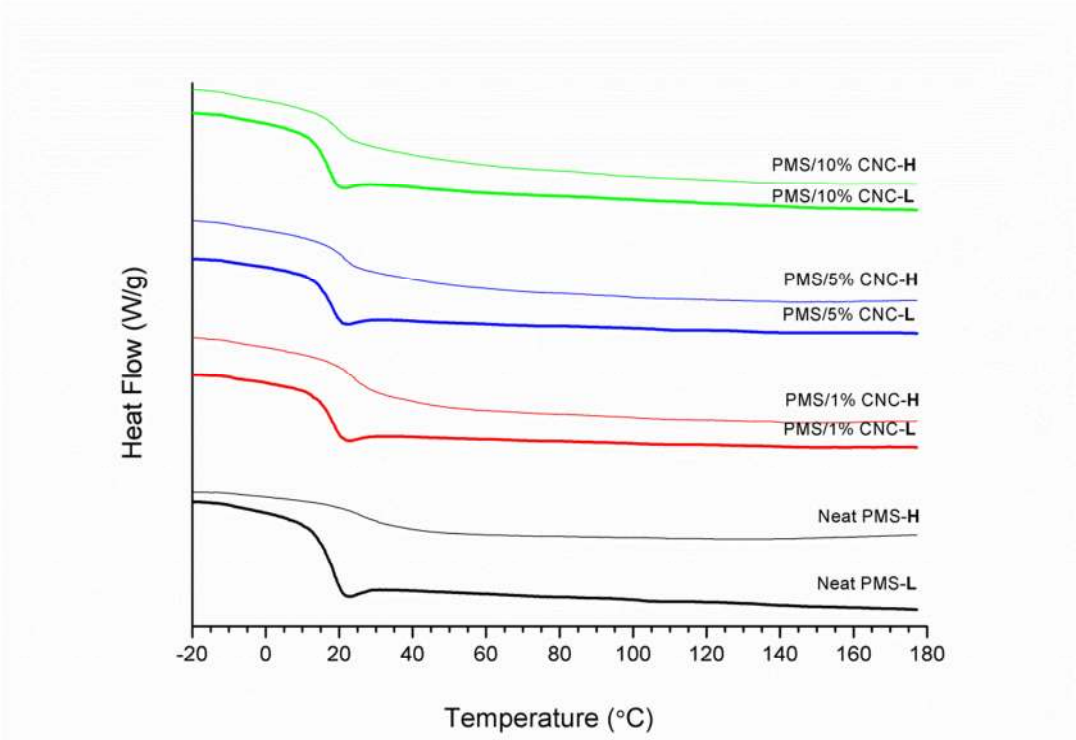

Figure S9. DSC second heating run thermograms of neat and nanocomposite samples with low **(L),** and high **(H)** degree of crosslinking.

References

1. E. N. J. Ford, S. K. Mendon, S. F. Thames, J. W. Rawlins, *J.Eng. Fiber Fabr.* **2010**, *5*, 10-20.

2. N. Terinte, R. Ibbett, C. K. Schuster, *Lenzinger Berichte* **2011**, *89*, 118-131.

3. M. Jorfi, M. N. Roberts, E. J. Foster, C. Weder, *ACS Appl. Mater. Interfaces* **2013**, *5*, 1517-1526.

4. A. C. Correa, E. d. M. Teixeira, L. A. Pessan, L. H. Capparelli Mattoso, *Cellulose* **2010**, *17*, 1183-1192.

5. S. Camarero Espinosa, T. Kuhnt, E. J. Foster, C. Weder, *Biomacromolecules* **2013**, *14*, 1223-1230.

6. I. Filpponen, D. S. Argyropoulos, *Ind. Eng. Chem. Res.* **2008**, *47*, 8906-8910.

7. H. Gottlieb, V. Kotlyar, A. Nudelman, *J.Org.Chem.* **1997**, *62*, 7512-7515.

8. Y. Li, J. A. Ragauskas, In Advances in Diverse Industrial Applications of Nanocomposites; Reddy B.; Eds.; InTech, 2011; Chapter 2, pp 18-36.

9. M. Samir, F. Alloin, J. Sanchez, A. Dufresne, *Polymer* **2004**, *45*, 4149-4157.